Journal of Electrical Engineering & Technology
https://doi.org/10.1007/s42835-026-02777-x

ORIGINAL ARTICLE

Fuzzy Logic-Based Control of a Battery Energy Storage System to Mitigate Frequency Excursions in the Cuban Power System Caused by Electric Arc Furnaces

Julio Espinosa Domínguez[1] · **Ioan Serban**[1] · **Orlys Ernesto Torres Breffe**[2]

Received: 24 April 2025 / Revised: 3 April 2026 / Accepted: 7 April 2026

Abstract
This paper proposes an adaptive control for a battery energy storage system (BESS) using a fuzzy logic controller (FLC), specially designed to operate in parallel with an electric arc furnace (EAF) in the Cuban power system. The BESS control system was developed with considerations for the characteristics of the Cuban power system, the typical power demand profile of the EAF, and the battery lifetime. The primary goal is to mitigate the frequency excursions that currently occur during EAF operation, enabling the furnace to complete the smelting process without restrictions. Furthermore, the system aims to reduce battery stress, thereby enhancing their lifetime. For this purpose, the BESS active power is managed by an adaptive compensator, governed by the FLC. Based on information coming from all three components involved - power system frequency, furnace state and battery usage rate, the proposed FLC generates an optimal output to adjust the compensator's behaviour. The performance of the proposed system was evaluated through simulations and experimental tests. The results demonstrate that using adaptive control applied to BESS can be an effective solution for steelworks connected to weak power systems, such as the current Cuban power system.

Keywords Battery energy storage system · Cuban power system · Electric arc furnace · Frequency · Fuzzy logic controller

1 Introduction

The development of mankind has been closely linked with the production of materials like steel, which requires a significant amount of energy to produce. The steel manufacturing process is extremely complex and begins with the selection and classification of scrap within the steelworks, followed by the smelting process and the introduction of chemical materials to produce high-alloy steels [1]. One stage of steel production is the smelting process, which takes place in steelworks using high-power electric arc furnaces (EAFs). Due to their operation characteristics, EAFs are highly demanding on power systems. EAFs cause power quality problems for the steelworks' electricity supply system, which must be mitigated to avoid impacting the nearby consumers [2, 3]. In addition to power quality issues, such as harmonic pollution, flicker, low power factor and imbalances, these high-power consumers can cause severe perturbations in the frequency of weak power systems [4, 5], such as the Cuban power system. In such cases, to avoid frequency stability problems, the power system operator may require limiting the power demand of EAFs, which can severely affect the efficiency of the steel production process [4]. It is important to note that the impact of EAFs on frequency is a major issue in the Cuban power system

✉ Julio Espinosa Domínguez
julio.dominguez@unitbv.ro

Ioan Serban
ioan.serban@unitbv.ro

Orlys Ernesto Torres Breffe
oetbreffe@yahoo.es

[1] Department of Electrical Engineering and Applied Physics, Faculty of Electrical Engineering and Computer Science, Transilvania University of Brasov, Eroilor 29, Brasov 500036, Romania

[2] Centre for Electroenergetic Research and Testing (CIPEL), Faculty of Electrical Engineering, Technological University of Havana, Street 114 No. 11901 Between Ciclovía and Rotonda, Havana 19390, Cuba

Published online: 28 April 2026

today, requiring different solutions compared to those used in strong grids such as the European power system [6].

One solution to frequency stability problems is the implementation of battery energy storage systems (BESS) in power systems [7–9]. The speed and effectiveness of the control systems of these devices help minimise frequency deviations, which is highly beneficial for conventional generation units that may not respond with the required speed. As the penetration rate of renewable energy sources (RES) increases, the frequency control process becomes more complex in all power systems, particularly in weak power systems [10, 11]. Therefore, the use of BESS is increasing significantly due to the numerous applications they have in power systems [12]. One popular application is the use of BESS to smooth RES power output [13], thereby enhancing the safe and reliable integration of RES into power systems. To achieve this, BESSs employ control methods to limit the power ramp rates. These methods employ compensators, such as linear low-pass filters (LPF), moving average filters, or exponential smoothing [13]. While effective RES power smoothing is achieved, one drawback of these smoothing techniques is their negative impact on the battery performance. Issues such as BESS battery overloading have prompted numerous studies in literature, aimed at addressing this challenge. These efforts explore more advanced control techniques leveraging fuzzy logic or artificial neural networks (ANN). Authors such as [14, 15] propose the implementation of fuzzy logic controllers (FLC) to smooth the power output of wind turbines and photovoltaic farms and to protect the battery lifetime, while works such as [16–18] use FLC to avoid battery ageing and to protect the battery from high continuous currents with high C-rates.

Other research suggests conducting feasibility studies on the performance of photovoltaic farms using fuzzy logic to determine the characteristics of the BESS to be installed, aiming to smooth the power output and reduce the ramp rate [19, 20]. Although these works have achieved good results, more recent research proposes the use of predictive control through neural networks to smooth the power output and optimize the battery charge levels [21, 22]. Based on the methods deployed for RES power smoothing, this paper explores the implementation of these solutions, opening a path to future industrial applications where the variability in loads such as EAFs could be minimised to improve power quality and production profiles.

To further emphasize the need for this research, a summary of the most relevant studies on the topic is provided in Table 1. Based on the literature review, the following gaps were identified:

1) Most studies address frequency control and battery life extension independently, without demonstrating a significant interrelationship between the two. Consequently, there is a need to develop more efficient BESSs in power systems that not only contribute to frequency control, but also intelligently manage battery usage to reduce maintenance costs.
2) The consideration of the *C-rate* in control systems to protect and reduce battery usage is insufficient, most studies focusing only on the state of charge. Incorporating this factor in real time, where feasible, could offer additional benefits by reducing the stress on the battery, thereby extending its lifetime.
3) The implementation of advanced controls in BESS for industrial loads that can affect power system stability is limited in most of the reviewed studies. Integrating the specific operation characteristics of EAFs, into BESS control systems would improve the efficiency of these industries while contributing to maintaining power system stability.

Research on BESS applications in EAFs has been limited mainly to improving power quality [24–26], while others such as [27, 28] have raised the possibility of using BESS to improve frequency stability in power systems. The main drawbacks of these applications are that they use BESS with high energy capacity and high C-rate values, which makes the application more expensive from a technical point of view. To address this issue, the aim of this paper is to propose a fuzzy logic-based adaptive control for a BESS, specially designed for operation in parallel with an EAF within the Cuban power system. The primary goal is to mitigate the EAF impact on the Cuban power system, thereby reducing the frequency deviations caused by these furnaces and ensuring the continuous operation of the steelworks. Furthermore, the proposed BESS control system aims to decrease the wear of the batteries. In addition, the control system should be adaptable to all stages of the steelworks production process, thus improving efficiency and production levels in the industry.

The main contributions of this paper are listed below:

Table 1 Reference summary of BESS with advanced control features

Reference	Advanced Control System Type	Considers frequency control	Extends battery life	Considers C-rate	Considers industrial loads
[14–16, 19]	FLC	✗	✓	✗	✗
[17]	FLC	✓	✓	✓	X
[21, 22]	ANN	✗	✓	✗	✗
[18]	FLC	✓	✓	✗	✗
[20, 23]	FLC	✓	✗	✗	✗
Proposed paper	FLC	✓	✓	✓	✓

- Development of a control system for a BESS adapted to the specific case of the EAF integration in the Cuban power system.
- Implement a fuzzy logic-based control system designed to reduce frequency deviations caused by EAF operation, while simultaneously keeping the battery use at minimum.
- Evaluate and experimentally validate the control system within the context of the Cuban power system.

2 Frequency Behaviour of the Cuban Power System During Operation of a High-Power EAF

The operation of high-power EAFs is not typical in weak power systems, which may present problems in the process of frequency regulation. As discussed in the Introduction, this is the case of the Cuban power system, which for various reasons today has problems with frequency regulation during the operation of EAFs [5, 6]. In this context, the system operator must control and limit the maximum power of the EAF to prevent potential loss of power system stability [4]. It is important to mention that the frequency control today in Cuba implies a dead band between 59.7 and 60.2 Hz, which is significantly higher than in other stronger power systems (±10 mHz in the European grids [29]).

Within this dead band, no restrictions are imposed to the EAF. However, due to the variable installed capacity of the Cuban power system, which also influences inertia and damping, these limits can be easily reached during the starting and stopping phases of the EAF.

The frequency behaviour of the Cuban power system associated with the operation of a 50 MW EAF during a normal day is shown in Fig. 1 (experimental measurements). Under these conditions, the EAF demand does not reach the full required power of 50 MW because the system operator imposes limits on the furnace power throughout the smelting process. Although the operation of the EAF is constrained by the system operator, the frequency still exceeds the dead band for several seconds during the entry and exit of the furnace, when the rate of EAF active power variation is high. This behaviour highlights the weakness of the Cuban power system in regulating the frequency under the influence of high-power EAFs.

Table 2 shows the general results of the frequency behaviour of the system. In addition to the maximum and minimum values of the frequency, the times during which the frequency exceeds the dead band during the operation of the EAF are also shown. Based on these results, it is evident that under current conditions, controlling the frequency during the operation of high-power EAFs poses significant challenges for the Cuban power system. Therefore, measures

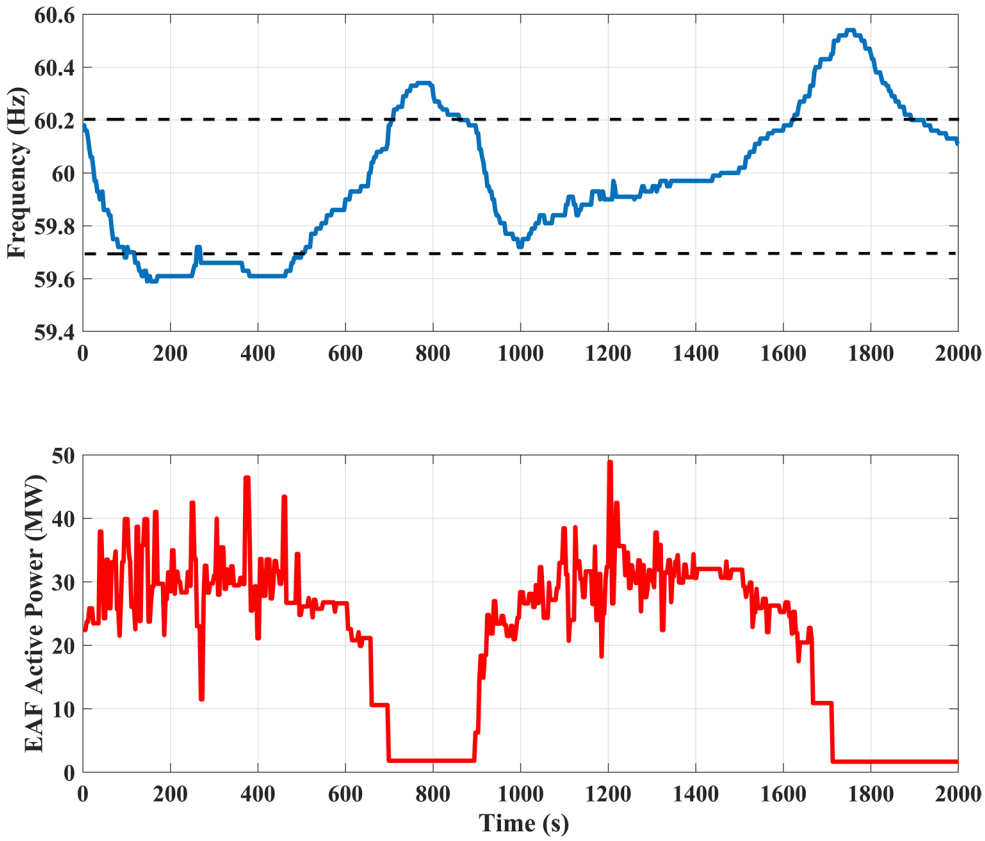

Fig. 1 Frequency response of the Cuban power system during operation of a 50 MW EAF (experimental measurements)

Table 2 Frequency behaviour of the Cuban power system under the action of a 50 MW EAF

Parameters	Values
Maximum frequency (Hz)	60.542
Minimum frequency (Hz)	59.591
Time above 60.2 Hz (s)	442
Time below 59.7 Hz (s)	403

must be implemented to minimize frequency deviations and ensure continuous operation of the steelworks.

Given the challenges outlined above, the objective of this paper is to design a control system for a BESS that mitigates large frequency deviations caused by EAFs operation in the Cuban power system. This control system should allow the continuous and efficient operation of the steelworks, together with the improvement of the useful life of the batteries, which would reduce the maintenance costs of the BESS to be implemented.

3 Use of a Low-Capacity BESS to Offset a High-Power EAF

The proposed solution to ensure the continuous operation of EAFs in the Cuban power system involves using BESSs in parallel with the EAF, as shown in Fig. 2. It is important to note that the main purpose of this system is not to control the power system's frequency directly. Instead, it aims to compensate for the rate of power change demanded by the furnace, thereby preventing strong frequency excursions that could jeopardize the stability of the Cuban power system, and thus keeping the EAF in operation [4, 5]. Nowadays, issues related to the weak frequency control of the Cuban power system during the EAF operation are partially addressed by enforcing the power ramp operation of the EAF, which is achieved by adjusting the tap changers of transformers. This method has a poor performance in terms of controllability and makes EAF operation inefficient. Moreover, if the frequency of the power system drops below a certain threshold during the EAF operation, the power system operator may require the EAF to reduce its power consumption (as was shown in the previous section) or even stop. This results in significant losses for this industry.

It is important to mention that, due to the specific characteristics of the Cuban power system, the steelworks have a direct connection to the high-voltage transmission network, as shown in Fig. 2. To avoid flicker, and other voltage-related power quality disturbances, the steelworks has undergone a grid reinforcement process by connecting two transformers in parallel, each rated at 125 MVA [4, 5]. Therefore, in the point of BESS connection (Bus 2), the short-circuit power ($S_{SC\text{-}Bus2}$) is around 2000 MVA. The high-short circuit power is favourable for the BESS connection in parallel with the EAF, as will be discussed in the next subsection.

The use of a BESS in parallel with the EAF would compensate for the high-power fluctuation rates generated by the EAF, and thus the BESS would help to reduce the impact on frequency. In the compensation process, the control system of the BESS plays a key role. This system is composed of inner and outer controls which are responsible for controlling the power output of the battery. A simplified diagram of the control loops involved in BESS control is shown in Fig. 3.

3.1 Control of BESS Converter

The nominal power of BESS was considered to be 25 MW, similar to that proposed in [4]. The aim of this idea is that the BESS and the power system each compensate for approximately half of the peak demand of the EAF, thus reducing the frequency deviations during the smelting process. The

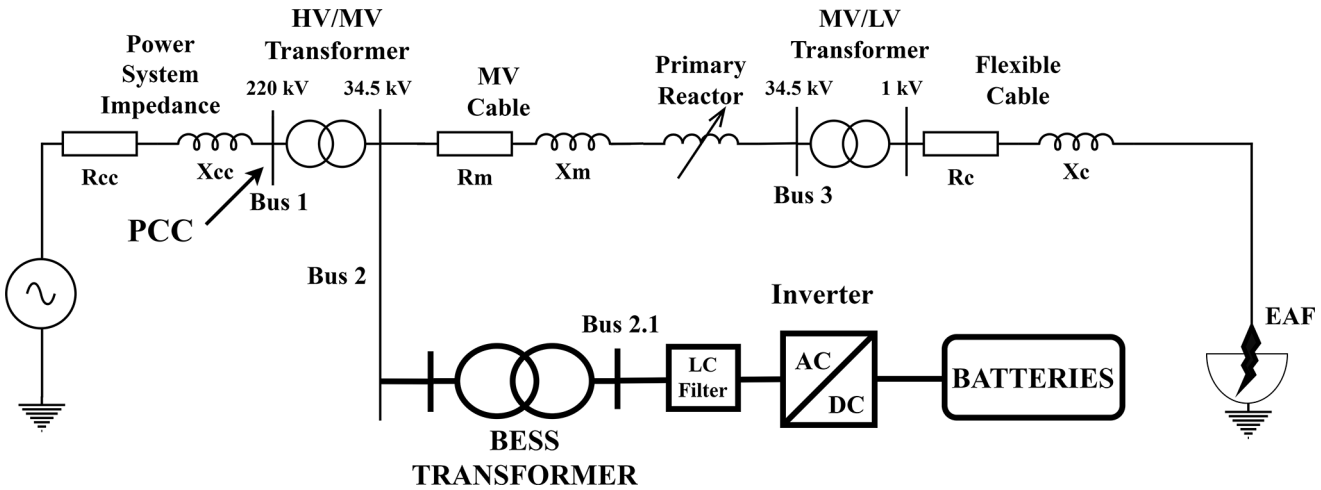

Fig. 2 Integration of a BESS into the circuit of an EAF

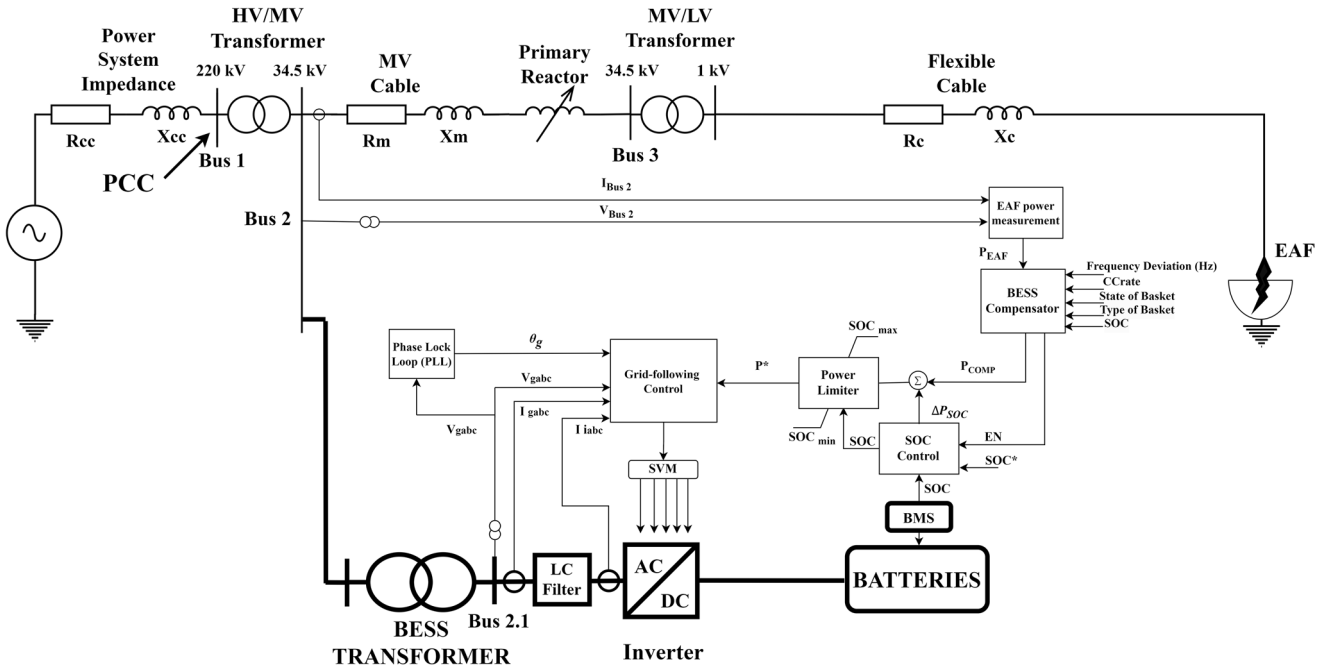

Fig. 3 BESS control block diagram

high short-circuit power level at Bus 2 ensures a stable voltage, as demonstrated in Sect. 3.3, which simplifies the selection of grid-connected control for the BESS inverter. As demonstrated in many studies, the short-circuit ratio (*SCR*) represents a key parameter in determining whether to use grid-following or grid-forming control for the inverter [30, 31]. The *SCR* at Bus 2 is defined as:

$$SCR_{Bus2} = \frac{S_{sc-Bus2}}{P_{r\_BESS}} \tag{1}$$

where, $S_{sc-Bus2}$ represents the three-phase short-circuit power (2000 MVA) on Bus 2 and P_{r_BESS} represents the rated power on the converter side of the BESS (25 MW).

The result shows an SCR of 80, which is significantly greater than the typical stability boundary of 4 used to determine the selection between the two control methods [30, 31]. Therefore, the grid-following (GFL) control is required in this case. Taking these considerations into account, the BESS control system depicted in Fig. 3 is designed around the inner GFL control. As shown, at Bus 2 current and voltage measurement sensors are placed to obtain the EAF power consumption. The calculated EAF power is used as a reference for the BESS compensator, which is responsible for compensating the EAF power according to the proposed method. This system consists of a filter that can be adaptive or not, depending on its configuration. The operation of the filter in conjunction with the EAF will be discussed in detail in the following sections.

The BESS control also includes a *SOC* controller that ensures the battery *SOC* to be restored to the reference value. To achieve this, a *SOC* compensation power (ΔP_{SOC}) is added to the reference power provided by the BESS compensator (P_{comp}). It is important to note that the *SOC* controller is activated only during the EAF's break periods to avoid interfering with the main BESS compensator. The *SOC* controller receives the *SOC* by means of the Battery Management System (BMS), and generates the signal ΔP_{SOC} based on the system conditions [32]. Furthermore, the reference power (P^*) of the BESS used by the inner GFL control is constrained by the limits set for the battery *SOC* ($SOC_{\min}$ and $SOC_{\max}$) to prevent overcharging or over-discharging.

The GFL control is shown in Fig. 4, where the internal current control loop provides the reference voltages to the space vector modulator that controls the BESS inverter. The goal of the internal current loop is to control the current flow through the inverter to follow the reference signal and contribute to the protection and power quality of the converter [31]. Additionally, there are two outer control loops, one for power control and another for low voltage ride-through (LVRT) control. All these controls were employed through a dq control strategy in conjunction with a phase-locked loop (PLL) to control the currents at the inverter output. In the case of the LVRT control, it is only activated when there is a low voltage in the network due to transient events, thus complying with the Cuban network code [6, 33]. The operation of this control loop superimposes the power control of the BESS and instead imposes the reference currents I_{dref_2} and I_{qref_2} on the current control. At the end of the

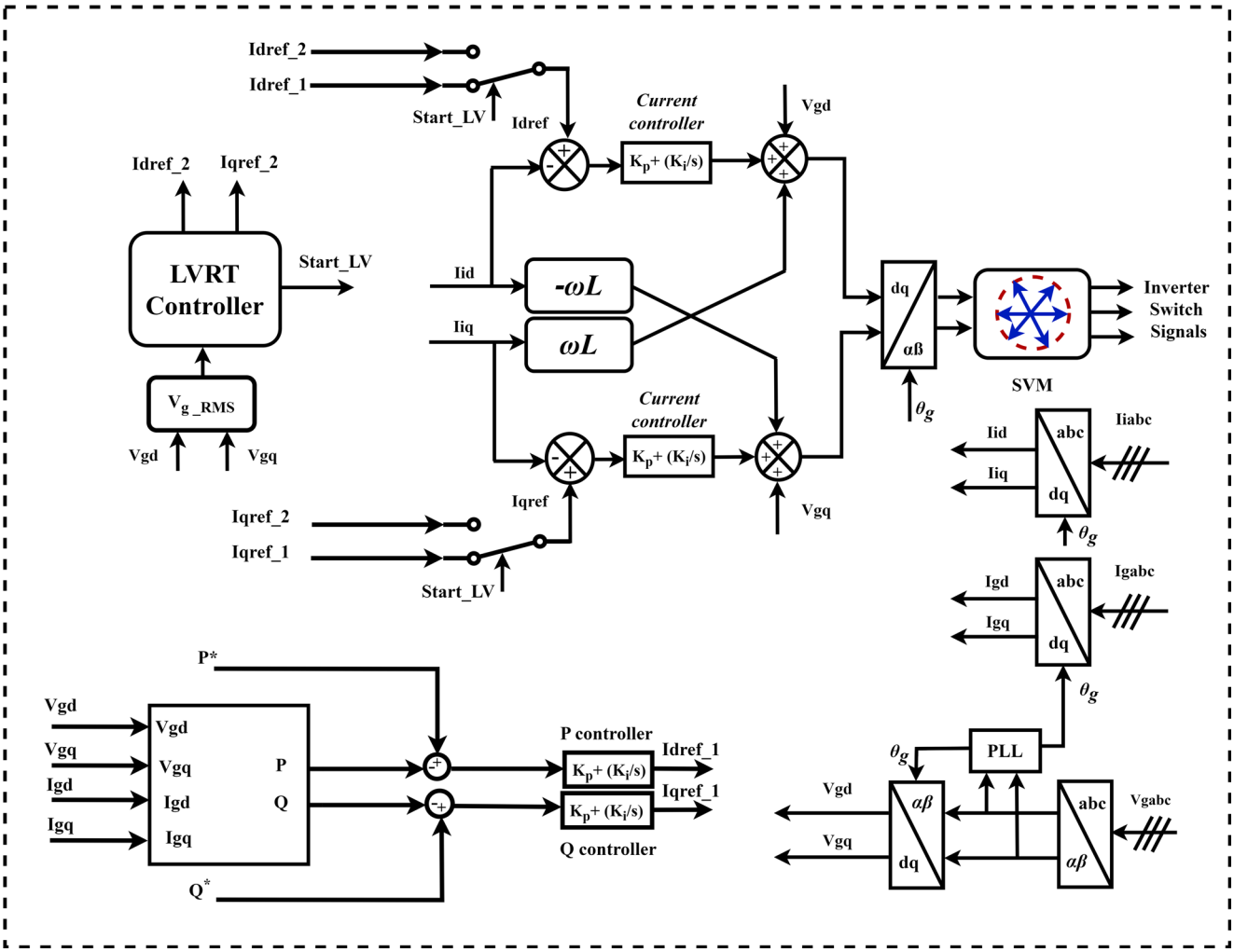

Fig. 4 BESS GFL control block diagram

process, when the mains voltage recovers, the LVRT control is switched off and the power control resumes. The description of the LVRT functionality is not included in this paper, as its analysis is beyond the scope of the present study.

It is important to note that at the MW power scale, BESS implementations typically employ multiple converters placed in parallel [34]. However, since this work focuses on the outer BESS control, specifically the compensator, a single equivalent converter is considered in Fig. 3.

3.2 Equivalent Power System Model for Analysing Frequency Behaviour

To analyse the frequency behaviour in the Cuban power system, an equivalent model was developed, as shown in Fig. 5 [35]. This allows replicating the previously described frequency behaviour, based on the parameters involved in frequency control - primary (λ_p) and secondary (K_s) control gains, along with the power system's inertia (H) and damping coefficient (D). This model will also be used in the experimental tests to emulate the power system.

The transfer functions describing the behaviour of the frequency in relation to the power variations, including the system response to a load change (G_1), primary and secondary control (G_2), are presented in (2) and (3). According to Fig. 5, the equivalent transfer function of the power system results as in (4).

$$G_1(s) = \frac{1}{2 \cdot H \cdot s + D} \tag{2}$$

$$G_2(s) = \lambda_p + K_s \cdot \frac{1}{s} \tag{3}$$

$$G_{ps}(s) = \frac{G_1(s)}{1 + G_1(s) \cdot G_2(s)} \tag{4}$$

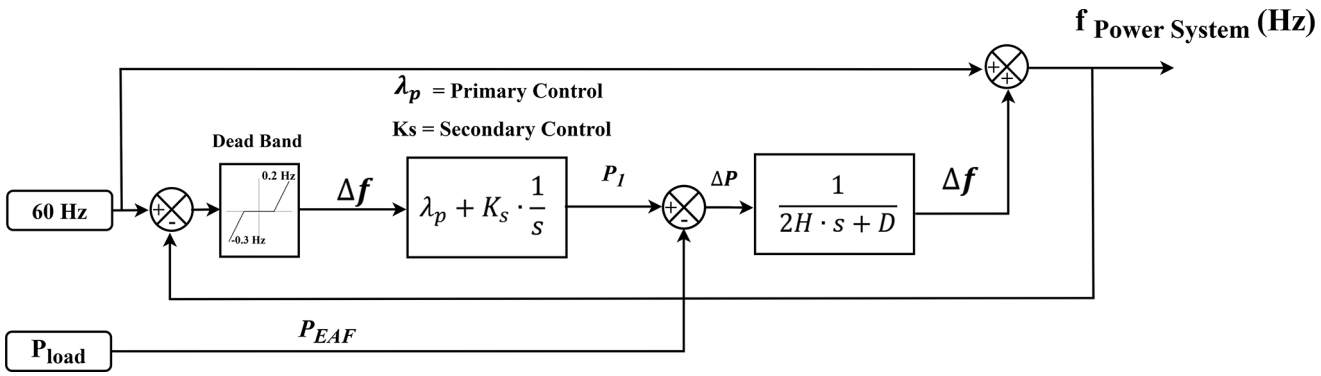

Fig. 5 Equivalent power system model for analysing frequency behaviour

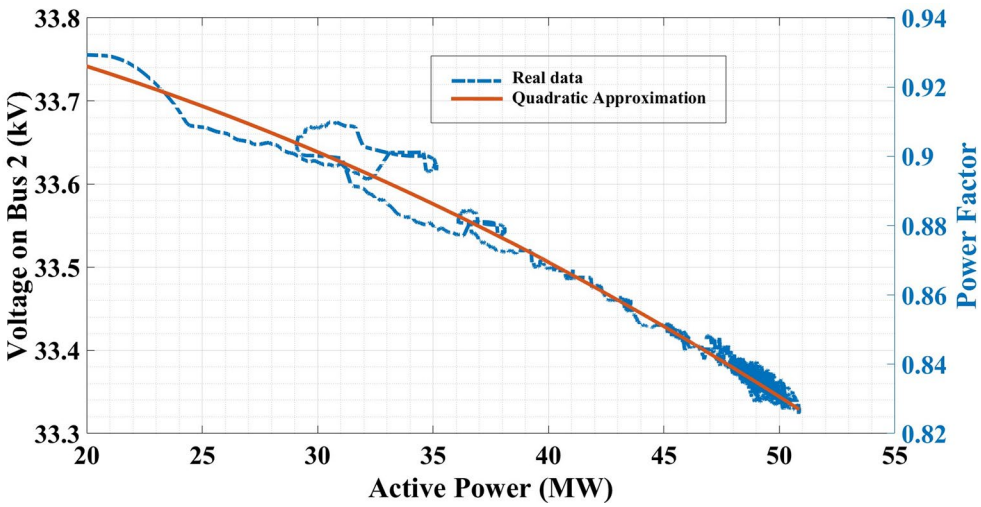

Fig. 6 Behaviour of Bus 2 voltage and power factor according to the power required by the EAF

The power variation that the system experiences due to the load demand and the power generated by the system (P_I) is introduced in the block that defines the dynamic characteristic of the system. The two specific parameters, inertia (H) and load damping (D) were obtained from a study of the conditions of the Cuban power system in recent years. The difference between the power system frequency and the reference frequency (60 Hz) causes an error in the output, which is responsible for activating the power system regulation controls when the dead band is exceeded. The activation of the regulation controls allows the influence of the primary and secondary control to be taken into account in the simulations, thus providing a more detailed analysis of the frequency behaviour of the Cuban power system. It is important to mention that currently, the primary and secondary control are weak, and the associated parameters can vary significantly according to the resources available in the power system.

3.3 Voltage Sensitivity to Power Variation on Bus 2

A voltage sensitivity analysis to the power variation on Bus 2 was carried out based on the analysis of a maximum load profile in the EAF. Figure 6 shows the variation of the voltage and power factor at Bus 2 as a function of the active power demanded by the EAF. Due to the variability of real data, it was necessary to use a quadratic approximation to represent the real behaviour obtained in the simulations. The derivative of the quadratic approximation reflects the sensitivity of the voltage in relation to the power variation [36], reaching in a maximum value of 0.013 kV/MW. This result indicates that the voltage exhibits a high stiffness and strength, meaning that load variations will have an insignificant impact on the BESS connected to Bus 2.

In general, the behaviour of the voltage profile shows that as the power required by the EAF increases, the voltage drop does not exceed 5% of the nominal value of 34.5 kV. This low voltage drop is further evidence of the voltage stiffness on Bus 2, calculated from expression (5) [37].

$$K_{vtg} = \frac{U_{sys}}{U_{sys0}} \tag{5}$$

where K_{vtg} is the voltage stiffness coefficient, U_{sys} is the voltage magnitude at full load, and U_{sys0} is the voltage magnitude at no load.

The voltage stiffness coefficient value was 0.988, indicating that the load connected to Bus 2 has minimal impact on the voltage magnitude. With this high stiffness, the connection of the BESS on Bus 2 will not be affected by the deterioration of the voltage magnitude.

4 Use of a Low-Capacity BESS to Offset a High-Power EAF

As shown in Fig. 3, the BESS active power reference is provided by a compensator that tracks the power variations of the EAF. The first implementation is based on a non-adaptive filter that has as input the active power of the EAF (P_{EAF}) measured in the point indicated in Fig. 3. This non-adaptive filter serves as the basis for developing the improved compensator, discussed in the next section.

Figure 7 shows the block diagram of the filter that uses the EAF power as an input. The action of the filter control loop is fundamental because it classifies the amount of power that the BESS will deliver to the power system. This filtering technique is one of many that are used to smooth the output power using a BESS; mainly in applications to control the variability of the output power of photovoltaic systems [13, 15, 19].

The transfer function of the LPF inside the compensator is given in (6), while the output of the filter is expressed in (7). The P* to be sent by the BESS to the power system is defined in (8), which represents a first-order high-pass filter. Note that the negative sign comes from the power sign convention used for controlling the BESS.

$$G_{LPF}(s) = \frac{1}{T_s s + 1} \tag{6}$$

$$P_{LPF}(s) = \frac{1}{T_s s + 1} \cdot P_{EAF}(s) \tag{7}$$

$$P^*(s) = P_{LPF}(s) - P_{EAF}(s) = \frac{-s}{s + 1/T_s} \cdot P_{EAF}(s) \tag{8}$$

The compensator performance will largely depend on the selected time constant T_s. As previously discussed, the inertia and damping of the Cuban power system are subject to significant and unpredictable variations. Therefore, selecting an optimal time constant for effectively control the EAF power and ensuring continuous operation becomes a challenging task. To evidence this, the next subsection analyses the performance of BESS under different power system conditions (inertia and damping).

Obtaining the transfer function in (8) shows the behaviour of the power that the BESS will inject or consume from the power system, which may have an influence on the stability. To evaluate the influence of the BESS on the power system, it is necessary to examine the relationship between the transfer function of the equivalent system and that of the BESS, shown in (9).

$$G_c(s) = G_{ps}(s) \cdot G_{BESS}(s) = \frac{G_1(s) \cdot G_{BESS}(s)}{1 + G_1(s) \cdot G_2(s)} \tag{9}$$

where $G_c(s)$ is the equivalent transfer function describing the relationship between the power system frequency variation and the power variation caused by the operation of the EAF, while $G_{ps}(s)$ and $G_{BESS}(s)$ are the transfer functions of the equivalent power system and the BESS first-order high-pass filter respectively. Substituting the terms of Eqs. (2), (3), (4) and (8) into (9) will result in the equivalent transfer function (10) in terms of the power system parameters and the time constant of the BESS filter.

$$G_c(s) = \frac{s^2}{2 \cdot H \cdot s^2 + (D + K_d + \lambda_p) \cdot s + K_s} \tag{10}$$

where H and D are the inertia and damping of the power system, λ_p and K_s are the primary and secondary frequency control constants respectively, and K_d is the inverse of the BESS filter time constant.

The quadratic equation of the denominator in Eq. (10) has two real solutions, since its discriminant is positive according to the parameters of the power system and the BESS. Analysis of these solutions shows that their real parts are negative, which, according to Lyapunov's first theorem, guarantees that the system is asymptotically stable [35]. These results also allow us to understand that changing the time constant of the BESS filter does not affect the stability

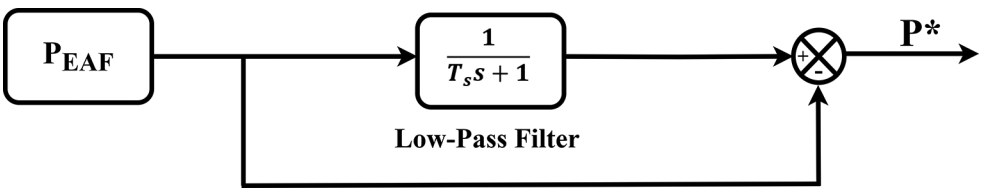

Fig. 7 Block diagram of the non-adaptive compensator

of the power system, since it behaves as an overdamped system even in the weakest conditions of the system.

4.1 Selection of the LPF Time Constant

The selection of this parameter depends on the intended BESS response during EAF operation. A high time constant would provide better BESS compensation, resulting in a lower EAF impact on the power system frequency. However, this will lead to higher usage of the battery, consequently increasing its wear [13]. Therefore, the optimal time constant will result from a trade-off between EAF's compensation performance and BESS's lifetime. However, because the parameters of the Cuban power system (total inertia, installed power) can vary significantly, this goal is difficult to reach with a fixed time constant. For this purpose, an adaptive filter will be proposed in the following section.

To determine the optimal time constant of the LPF, the following performance indicators were considered the integral of the absolute frequency error (IAE), as defined in (11), and the energy cycled by the BESS in a melting process, as defined in (12). From these indices, the optimal time constant of the filter (T_s) was determined for the weakest states of the Cuban power system, characterised by an inertia of $H = 58$ MWs^2/rad and a damping of $D = 25$ MW/rad/s.

$$IAE = \int_0^T |e(t)|\, dt \tag{11}$$

$$E_{BESS} = \int_0^T |P_{BESS}(t)|\, dt \tag{12}$$

where $e(t) = \Delta f(t)$ is the error of the power system frequency (frequency deviation from nominal), P_{BESS} is the power output of the BESS battery during the smelting process, and T is the duration of the melting process.

The results obtained under the above conditions are shown in Fig. 8. For this analysis, T_s was adjusted within a range to determine its optimum value, ensuring that the frequency remained within the specified limits during EAF operation. As shown in Fig. 8, increasing the filter time constant reduces the absolute frequency error, but this results in an increase in the energy processed by the BESS. For this reason, the optimum value of T_s was considered around the intersection of the two curves, resulting in a value between 140 and 150s. Therefore, a value of $T_s = 150$s was chosen as a reference for the proposed adaptive method described in the following section.

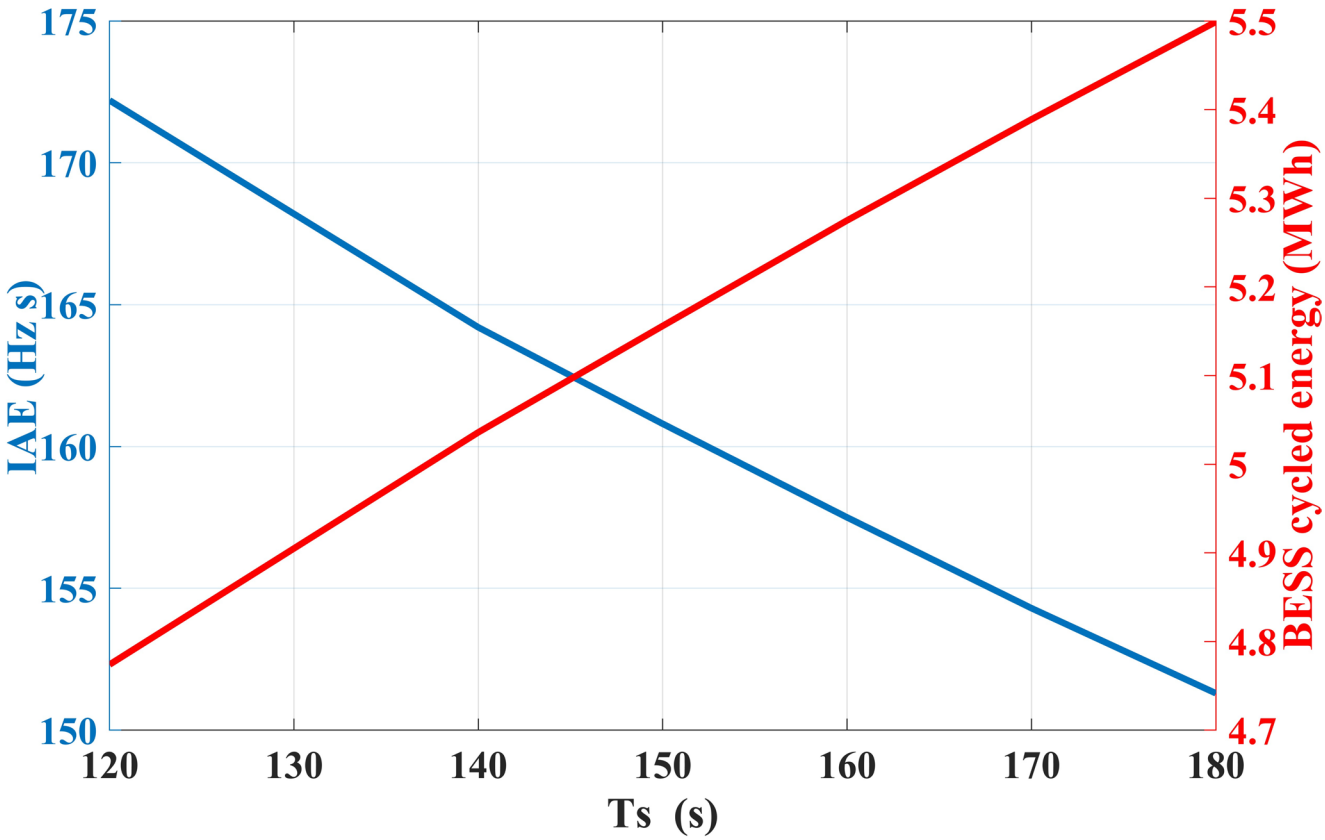

Fig. 8 Relationship between *IAE* and BESS cycled energy for different filter time constant values

4.2 Case Studies with Different Power System Parameters

To analyse the BESS compensation capability under different power system conditions, several performance indices were employed to characterize both the power system and the BESS battery usage. The indices that were used to analyse the behaviour of the power system were the frequency deviations and the maximum rate of change of the frequency ($RoCoF_m$) defined as [38, 39]:

$$RoCoF_m = \frac{f(t_0 + T) - f(t_0)}{T} \tag{13}$$

where $f(t_0), f(t_0 + T)$ are two consecutive frequency measurements and T is the time between two measurements, typically defined in grid codes (for the purpose of this research, T=0.5 s).

On the other hand, to evaluate the battery usage behaviour, the power output of the BESS, the energy consumed during the charging and discharging processes, the number of full cycles equivalents per year (FCE/a) defined in (14) and (15), the variation of the state of charge (ΔSOC) during the process defined in (16) and the average value of the C-rate curve, defined as the cumulative C-rate ($CC_{rate}(t)$) in (17), were observed.

The value of FCE related to the lifetime of the battery is determined by the equation given in [40]:

$$FCE = \frac{\sum_k |E(t_k)|}{2C} \tag{14}$$

where $E(t_k)$ is the total energy during a battery operation cycle and C is the battery capacity. For the evaluation of (FCE/a) in (15), it is assumed that the load profile is repeated an average of 15 times during the 260 working days of a year.

$$FCE/a = \frac{\sum_k |E(t_k)|}{2C} \cdot 15 \cdot 260 \tag{15}$$

The variation of the SOC can be expressed as:

$$\Delta SOC = SOC_{max1} - SOC_{min1} \tag{16}$$

where SOC_{max1} and SOC_{min1} are the maximum and minimum values of the battery charge during one cycle of EAF operation respectively.

The $CC_{rate}(t)$ indicates the relation between the maximum power of the BESS and the working time of the battery. The higher this rate, the longer the battery will consume or deliver power close to its maximum value. The values of the $CC_{rate}(t)$ are expressed in per unit values based on the nominal battery C-rate of 2.5:

$$CC_{rate}(t) = \frac{1}{T_f s + 1} \cdot \frac{|P_{BESS}|}{E_{r\_BESS}} \cdot \frac{1}{2.5} \tag{17}$$

where P_{BESS} is the power output of the BESS battery, E_{r_BESS} is the rated capacity of the battery and T_f is the time constant of a low-pass filter used to average P_{BESS} over a convenient window.

The use of a first-order filter in (17) allows the trend of the battery C-rate to be known to avoid high variations in the measurement. The increase or decrease in the cumulative C-rate gives a measure of the battery usage during the EAF compensation process.

Furthermore, to quantify the battery usage over one cycle of the EAF operation, the average cumulative C-rate value is defined as follows:

$$ACC_{rate} = \frac{1}{T_c} \int_0^{T_c} CC_{rate}(t) \cdot dt \tag{18}$$

where T_c is the time of one EAF cycle, and $CC_{rate}(t)$ is the cumulative C-rate defined in (17).

In order to test the effect of the proposed solution in the EAF compensation process, three case studies have been developed for different power system conditions. The compensator used in the BESS has a defined time constant of 150 s, as discussed previously.

The defined power system parameters are selected for different values of inertia and load damping. Case study 1 presents values of inertia (H=58 MWs^2/rad) and damping (D=25 MW/rad/s) that are very similar to the current weaker conditions of the Cuban power system, unlike the other values that were estimated as future scenarios where the power system conditions would be more robust. The future scenarios, called Cases 2 and 3, present inertia values of 58 MWs^2/rad and 100 MWs^2/rad, while the damping values are 50 MW/rad/s and 100 MW/rad/s, respectively. The use of the different conditions within the power system will allow the effect of the LPF to be characterised in detail.

The results of the different simulations (Fig. 9) show the frequency behaviour of the power system, BESS active power, active power behaviour of the power system, as well as the behaviour of the cumulative C-rate throughout the process. Table 3 shows the overall results of the simulations, where the base value for the representation of the active powers in p.u. was 50 MW. At the beginning of the simulation, before 200 s the BESS supplies a small amount of power to balance the EAF demand, which is in the arc ignition phase until stabilization, at which point the power demand increases. At t=1500 s, the EAF demand drops abruptly to a minimum due to the completion of the basket melting, which requires the BESS to be charged quickly to compensate in the power system for the rapid change caused by the load. In general, the BESS maintains the electrical

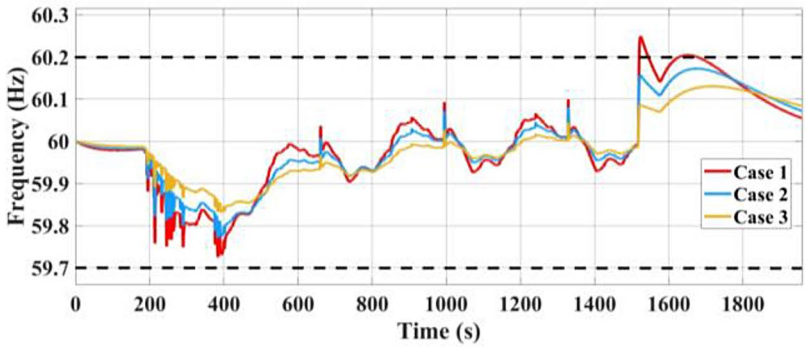

a)

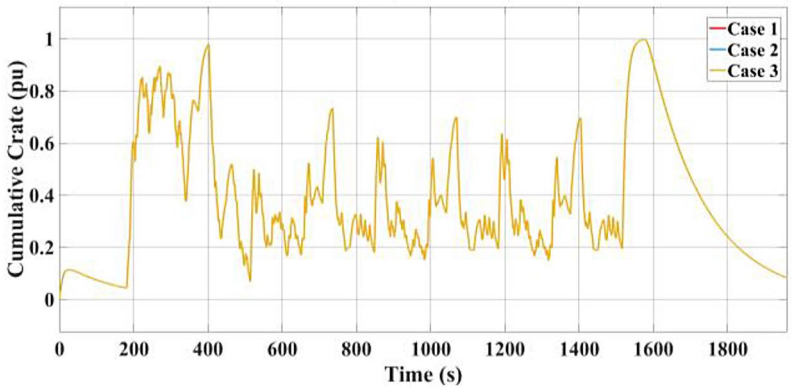

b)

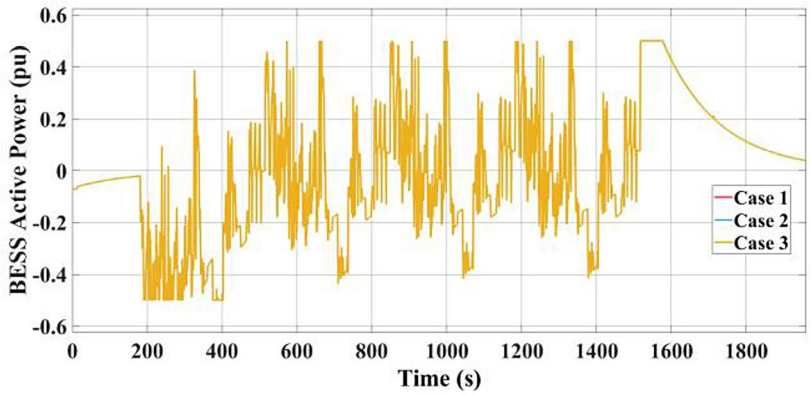

c)

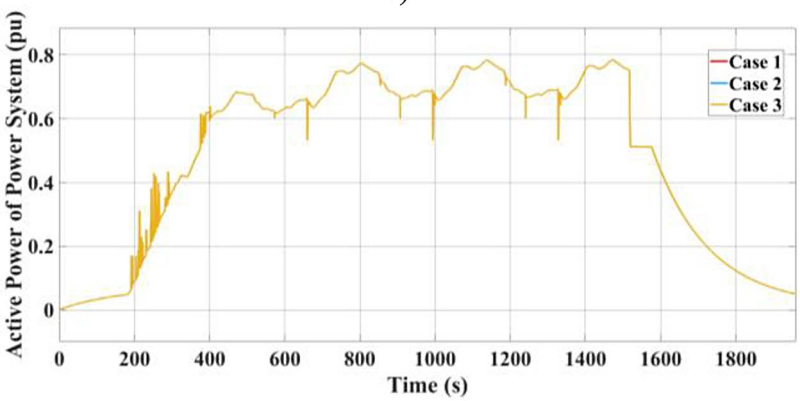

d)

Fig. 9 System operation with a non-adaptive compensator (T_s = 150 s): (**a**) frequency of the power system, (**b**) cumulative *C-rate*, (**c**) BESS active power, (**d**) active power behaviour of the power system

Table 3 Overall performance analysis with BESS including non-adaptive compensator (T_s=150 s)

Parameters	LPF with Ts = 150 s		
	Case 1	Case 2	Case 3
Average power (pu)	0.196	0.197	0.196
Maximum frequency (Hz)	60.248	60.172	60.130
Minimum frequency (Hz)	59.722	59.770	59.832
Time above 60.2 Hz (s)	66.612	0	0
Time below 59.7 Hz (s)	0	0	0
Average cumulative C-rate (pu)	0.384	0.385	0.384
Charge Energy (MWh)	2.632	2.632	2.632
Discharge Energy (MWh)	2.795	2.795	2.795
FCE/a	1058	1058	1058
ΔSOC (%)	16.82	16.82	16.82
$RoCoF_m$ (Hz/s)	0.097	0.090	0.052

frequency within the dead band under various power system conditions, as well as $RoCoF_m$ values within the security thresholds of the various international standards [38, 39]. To achieve this, the system delivers a significant amount of energy throughout the process to compensate for the EAF power variations. This is reflected battery's performance, where the cumulative C-rate in Fig. 9b illustrates that, during the beginning and the end of the process, the BESS charges at a high C-rate, which can lead to accelerated degradation. In addition, the BESS response with a non-adaptive compensator is limited and inefficient as the response is always maximum regardless of the state of the grid. In all three case studies, the power of BESS, the active power of the power system and cumulative C-rate values remained approximately constant, which means that the battery can be overworked in conditions where the power system is more robust. In terms of battery charging and discharging energy, full cycles equivalents per year and state of charge variations, the behaviour is similar in the three scenarios, showing once again that the compensator based on the fixed time constant filter does not allow the BESS to adapt to the varying conditions that frequently occur in the power system and in the behaviour of the EAF. Consequently, an adaptive compensator was developed to adapt to changes in grid conditions and EAF operation characteristics while minimizing battery wear. The next section presents the design of an adaptive filter based on fuzzy logic, which considers three fundamental elements: the power system, the EAF, and the BESS batteries.

5 Implementation of a Fuzzy-Logic Adaptive BESS Compensator

The previous results showed how a BESS can compensate for the power required by an EAF to avoid large grid frequency deviations. Although the use of a non-adaptive filter is one of the most widely used techniques by researchers due to its low complexity, it has the disadvantage that by using a fixed time constant (T_s) defined by the user, it can cause overloading of the BESS battery, which is reflected in a reduction of its useful life [13]. Based on these drawbacks, several authors have studied different adaptive techniques to extend the battery life. Among these techniques is the use of a fuzzy controller to select the time constant of an LPF in applications to smooth the power output of photovoltaic systems [13–15]. Although these adaptive techniques have shown how to reduce the overloading of BESS batteries, they have only been applied to RES systems and there is currently no record of works in the literature related to applications in EAFs. For these reasons, this work develops an adaptive control based on the application of fuzzy logic to select the time constant of an LPF used to compensate for the output power of an EAF in a weak power system, particularly the Cuban power system (Fig. 10).

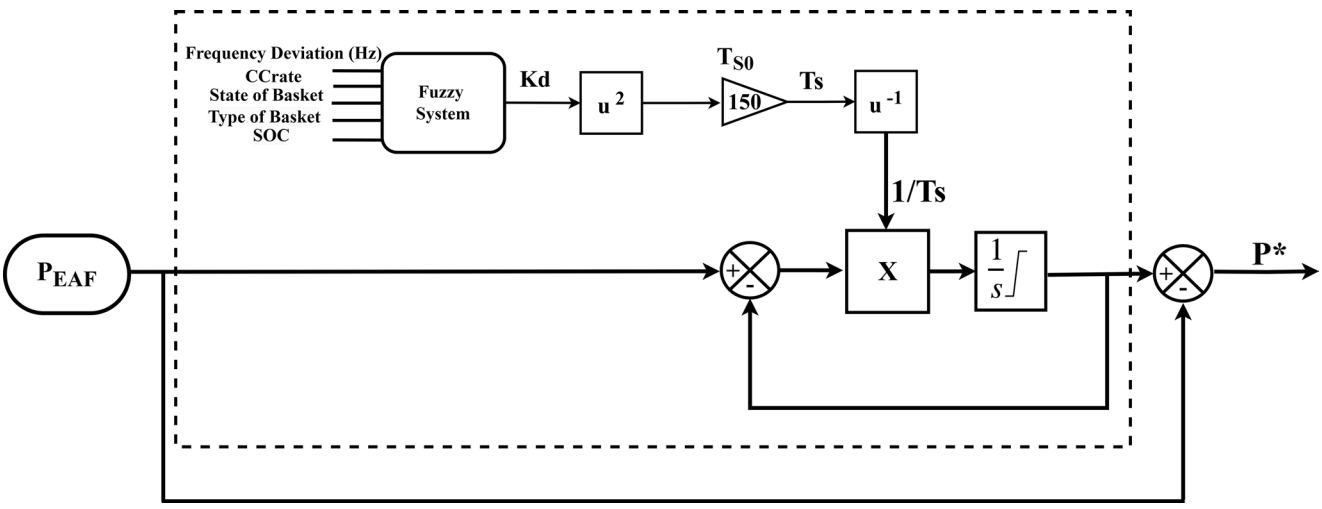

Fig. 10 Block diagram of the BESS compensator with FLC

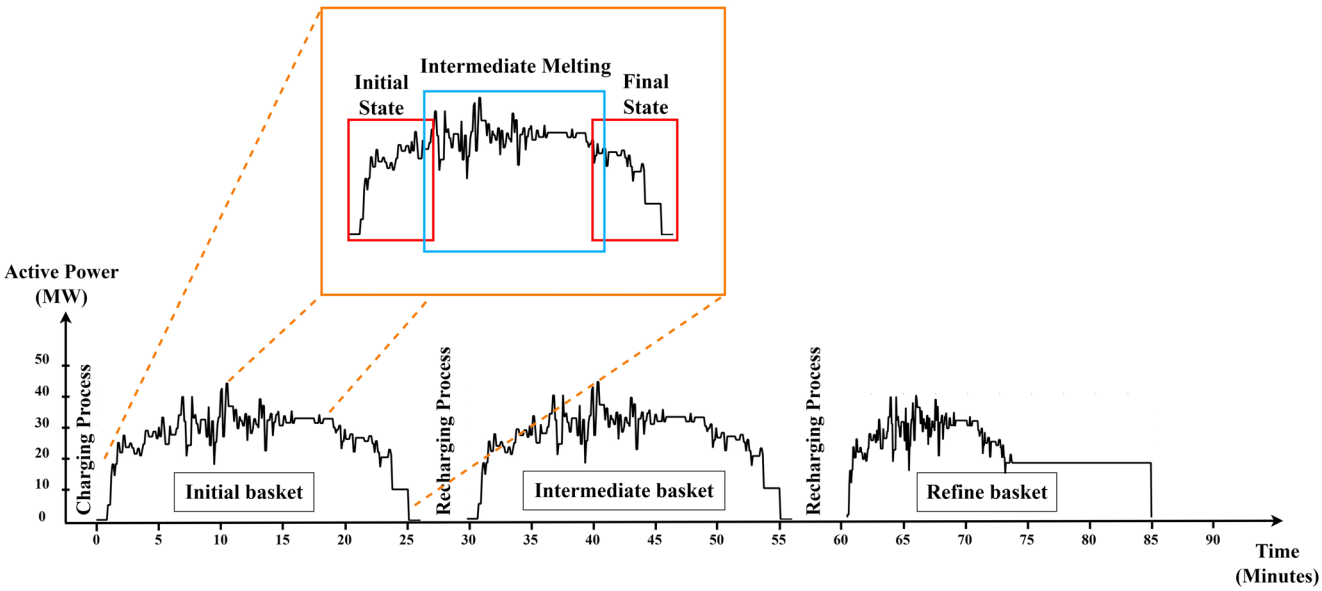

Fig. 11 Process of typical EAF operation

As shown in Fig. 10, the input variables to the fuzzy controller will be the frequency deviation (Δf), the cumulative C-rate of the battery, the state and type of the EAF basket that is melting and the SOC. The input variables describing the operation of the EAF are mainly based on its operation cycle (Fig. 11), which is divided into three phases: charging, melting and refining. During operation, the EAF is typically charged with three baskets: an initial basket, which contains the largest amount of scrap to melt; an intermediate basket, and a refining basket, which has the smallest capacity and requires less power. The total processing time for each basket varies between 20 and 30 minutes, during which time the state of the basket changes [41]. All these variables are aimed at obtaining the most efficient output of the FLC, which will have the least effect on battery life and will not allow the system frequency to reach unacceptable values outside the dead band for long periods.

In this research, the application of the adaptive filter time constant has been designed from a fixed time constant, which can change its value depending on the existing conditions in the power system and the EAF. This behaviour allows the time constant to be modified over a range of values greater or less than the fixed time constant. The relationship between the adaptive and fixed time constant is expressed in (19).

$$T_s = {K_d}^2 \cdot T_{s0} \tag{19}$$

where T_s is the adaptive constant of the filter, K_d is the FLC's output variable, and T_{s0} is the fixed constant, in this study considered equal to 150 s as discussed previously.

Figure 12 shows the surface plots of the relationship between the FLC's input and output variables. The value of K_d increases when the frequency is outside the dead band, although the value of this coefficient can be reduced depending on the EAF's basket type, the cumulative *C-rate* and the *SOC*.

The relationship between the input variables and the output of the fuzzy controller can be observed through a table of rules based on the IF-THEN format. To implement the rule set, the membership functions of the input and output variables have been defined and are shown in Table 4, Figs. 13, and 14.

Three membership functions for frequency deviation were considered: a Z-shaped function to represent the low frequency outside the dead band linguistic variable (*LF*), a generalised bell-shaped function for the normal frequency inside the dead band linguistic variable (*NF*), and an S-shaped function for the high frequency outside the dead band linguistic variable (*HF*). The second input variable, CC_{rate}, is composed of two membership functions: the first is a Z-shaped function representing the normal cumulative *C-rate* below 0.3 linguistic variable ($N\text{-}CC_r$), and the second is an S-shaped function describing the high cumulative *C-rate* above 0.3 linguistic variable ($H\text{-}CC_r$). The third input variable, state of basket, has three membership functions: the first is a Z-shaped function for the initial state linguistic variable (*IS*), the second is a generalised bell-shaped function representing the Intermediate melting linguistic variable (*IM*), and the third is an S-shaped function for the final state linguistic variable (*FS*). The fourth input variable, type of basket, is composed of three membership functions: the first is a Z-shaped function for the initial basket linguistic variable (*IB*), the second uses two Gaussian functions to represent the normal or intermediate basket linguistic variable (*NB*), and the third is an S-shaped function defining the refine basket linguistic

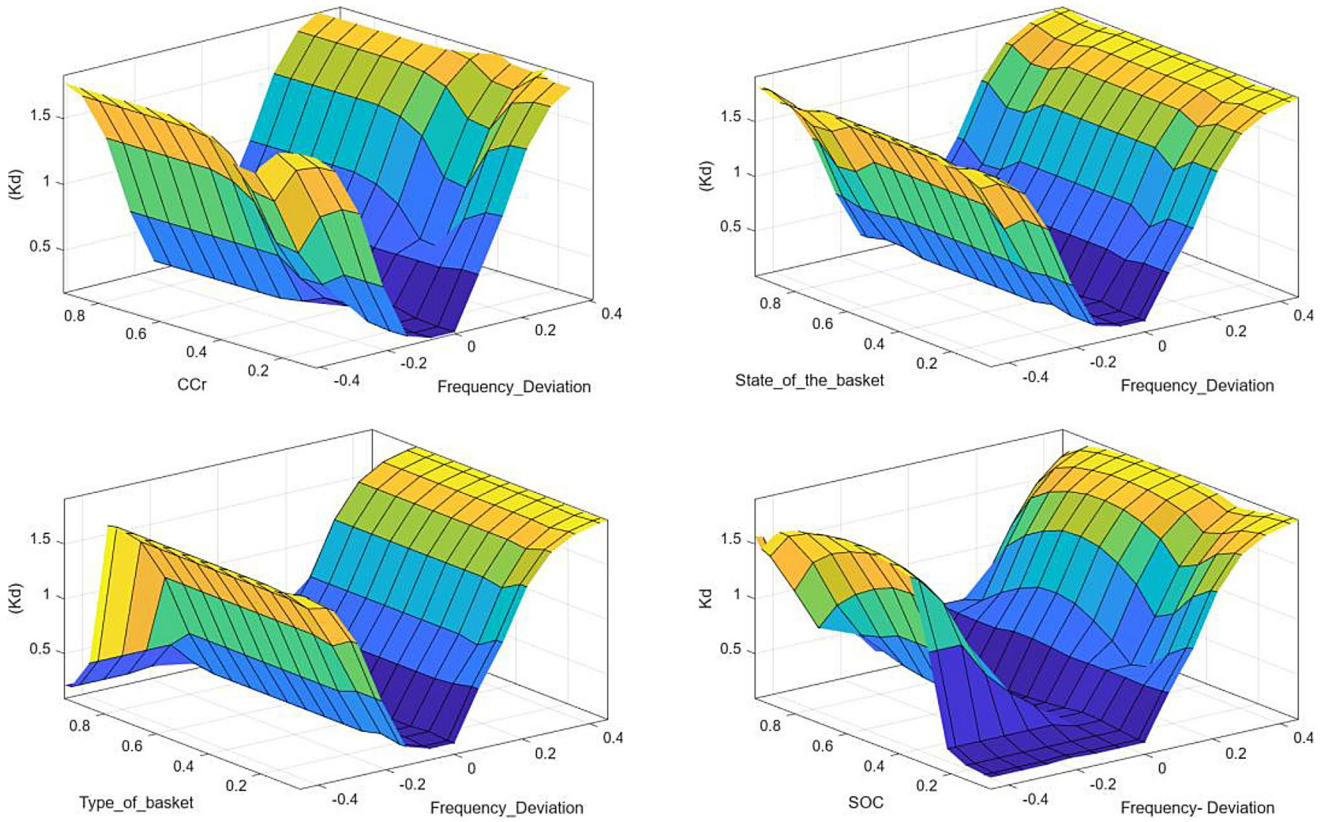

Fig. 12 Surface plots showing the relationship between the input variables and the output adaptive variable

Table 4 Fuzzy controller membership functions

Variable Name	Type of Variable	MF 1	MF 2	MF 3
Frequency Deviation	Input	*LF*	*NF*	*HF*
CCrate	Input	*N-CCr*	*H-CCr*	-
State of the Basket	Input	*IS*	*IM*	*FS*
Type of Basket	Input	*IB*	*NB*	*RB*
SOC	Input	*L*	*M*	*H*
Kd	Output	*HKd*	*LKd*	-

MF: Membership Function

where:

LF: Low frequency outside the dead band; *NF*: Normal frequency within the dead band; *HF*: High frequency outside the dead band; *N-CC$_r$*: Normal cumulative C-rate below 0.3; *H-CC$_r$*: High cumulative C-rate above 0.3;*IS*: Initial state; *IM*: Intermediate melting; *FS*: Final state; *IB*: Initial basket; *NB*: Normal or intermediate basket; *RB*: Refine basket; *L*: Low state of charge; *M*: Medium state of charge; *H*: High state of charge; *HKd*: High K_d coefficient; *LKd*: Low K_d coefficient

variable (*RB*). The fifth input variable, the *SOC* of battery, is composed of three membership functions: the first is a triangular function for the linguistic variable low state of charge (*L*), the second uses a triangular function to represent the linguistic variable medium state of charge (*M*), and the third is a triangular function defining the linguistic variable high state of charge (*H*). Finally, the output variable, coefficient K_d, is characterised by two membership functions: the first is a Z-shaped function for the Low K_d coefficient linguistic variable (LK_d) and the second is an S-shaped function for the High K_d coefficient linguistic variable (HK_d).

The membership functions are fundamental in the design of the adaptive controller rules. These rules were designed to consider both the knowledge of the EAF production process and the frequency control of the power system. Furthermore, they were designed to optimise the use of the battery, ensuring its efficiency without compromising its lifetime. A summary of the main FLC rules that determine the degree of battery utilisation is shown in Fig. 15.

To test the proposed adaptive control, three case studies with the previously define power system conditions (inertia and damping) were simulated. The simulation results (Fig. 16) show the behaviour of the power system frequency, BESS and power system active powers, as well as the variation of the cumulative *C-rate* throughout the process. In addition to these variables, Fig. 16e shows how the time constant is changed by the fuzzy controller in the three cases, while Table 5 synthesises the overall results. Similar to the use of the non-adaptive compensator, at the beginning of the simulation it is noted that the BESS compensates for the power required during the arc ignition phase before $t=200$ s. Then, after $t=1500$ s, the BESS starts charging at a high rate to stabilise the power system following the EAF disconnection.

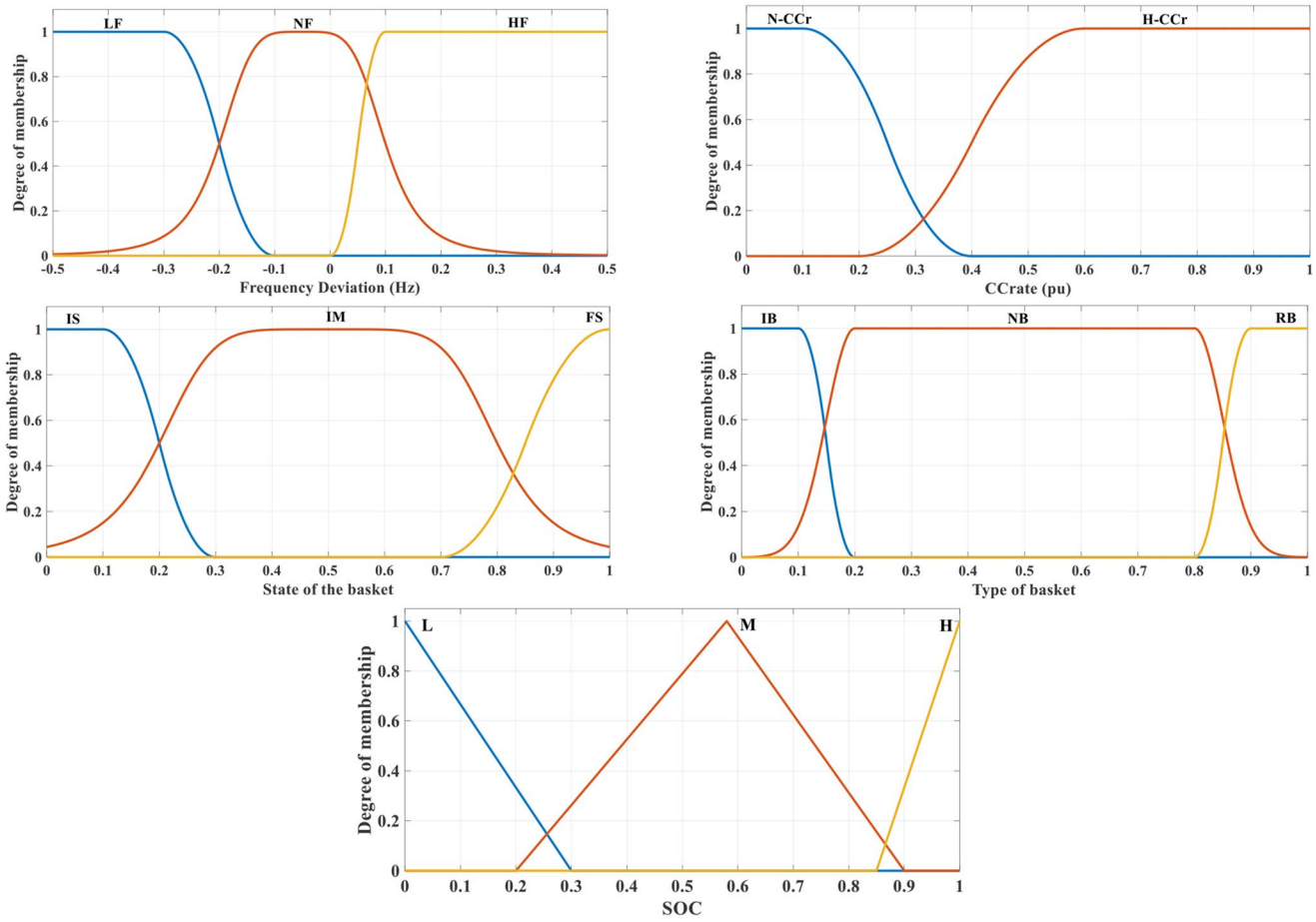

Fig. 13 Membership functions of input variables

Fig. 14 Membership function of the output variable

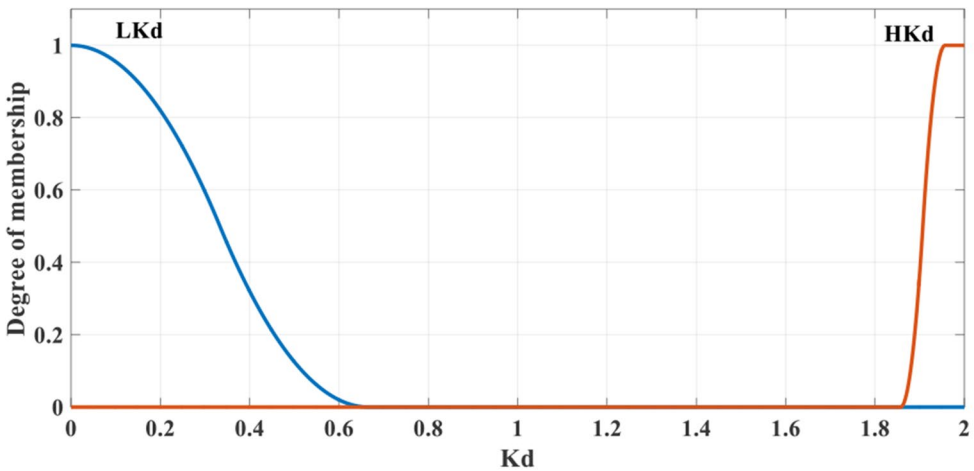

As shown, the FLC keeps the frequency within the dead band in the different conditions of the power system, as well as $RoCoF_m$ values within the security thresholds of the various international standards [38, 39]. Unlike the case with a non-adaptive compensator, the proposed controller makes it possible to reduce the average output power of the BESS without compromising the stability of the power system during the EAF operation.

To achieve optimum performance, the controller continuously varies the value of the LPF time constant to select the best response to the BESS output. Initially, the time constant is maintained below the reference value of 150 s, while

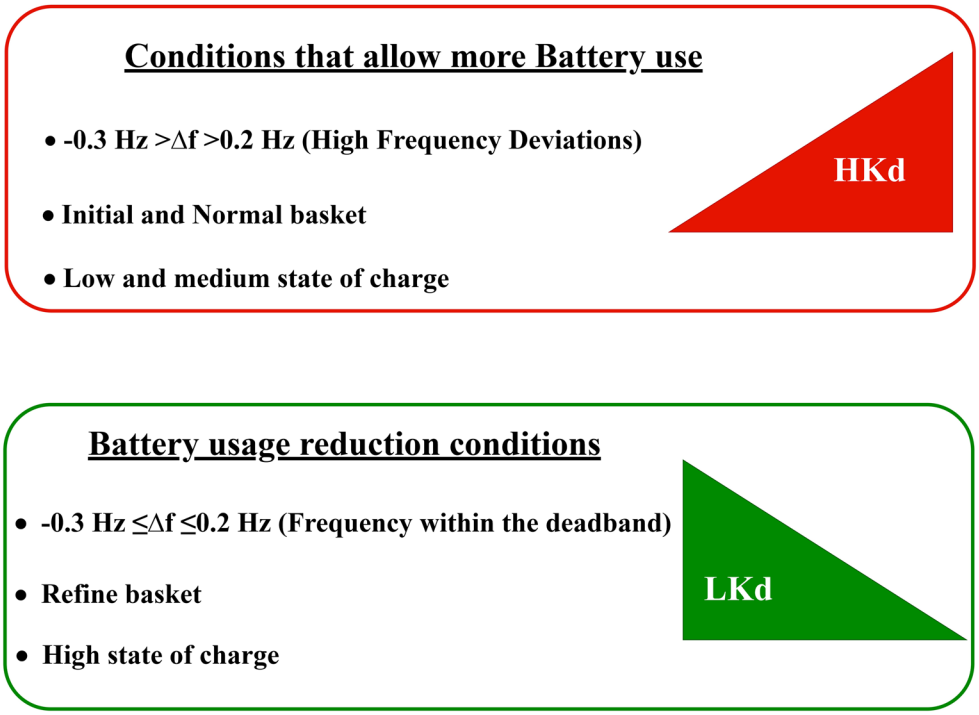

Fig. 15 Conditions that indicate higher or lower battery usage

towards the end of the process, it becomes necessary to increase the time constant above this threshold. This adjustment is required due to the abrupt power reduction of the EAF, which induces the frequency deviation, limited by the fast action of the BESS.

Regarding the CC_{rate} variation across the three case studies, it decreases as system conditions improve. This behaviour is also reflected in the BESS output power, which decreases as the system becomes more robust (Case 2 and 3), better meeting the EAF power demand. In terms of battery charging and discharging energy, the behaviour decreases as the power system conditions improve, even though the charging process consumes the most energy due to the abrupt power reduction of the EAF. In addition, the full cycles equivalents per year and state of charge variations decrease with improved grid conditions, meaning that this control system helps to extend battery life.

In general, the behaviour of the adaptive control allows the work of the BESS battery to be reduced as the power system conditions improve, thus avoiding accelerated battery degradation. In addition, unlike LPF with a fixed time constant, adaptive control allows to consider not only the power system conditions but also the state of the EAF in conjunction with the working conditions of the BESS, making it a more general and efficient control strategy.

5.1 Comparative Analysis of the Different Controls Used in BESS

The use of different control systems in the EAF demand compensation process leads to differences in battery usage throughout the process. These differences require a comparative study to analyse the advantages and disadvantages of each control system.

Table 6 shows the comparisons of the results obtained by each control system. The variables analysed were grid frequency, average output power, time out of dead band, cumulative battery *C-rate*, the charging and discharging energy of the battery, the number of full cycles equivalents per year, the maximum rate of change of the frequency and, the variation of the state of charge.

The results in Table 6 show that the use of an adaptive system reduces the average power injected to compensate for the EAF. Additionally, the cumulative *C-rate* is significantly lowered, along with the full cycles equivalents per year and state of charge variations. Therefore, the results show that the proposed BESS solution enhances the EAF operation in the conditions of the Cuban power system while achieving a trade-off between performance and minimal battery usage.

Regarding the times when the frequency is outside the dead band, it can be said that the use of an LPF with a fixed time constant allows the frequency to be inside the dead band most of the time during the smelting process, although, in the conditions where the power system is weakest, the frequency is outside the dead band for about 67 s. While the adaptive filter only allows the frequency to exceed the upper limit of the dead band for about 33 s in the weakest system conditions, it never allows the frequency to fall below the lower limit of the dead band, which poses greater challenges for the power system due to a generation deficit in the power system.

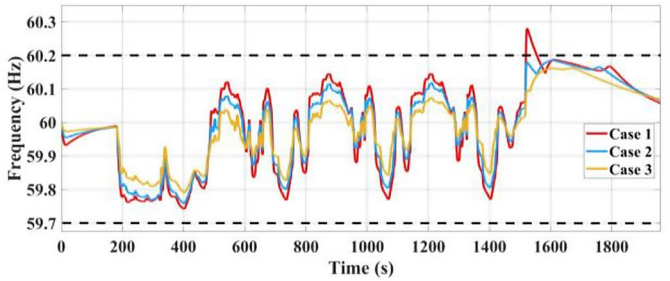

a)

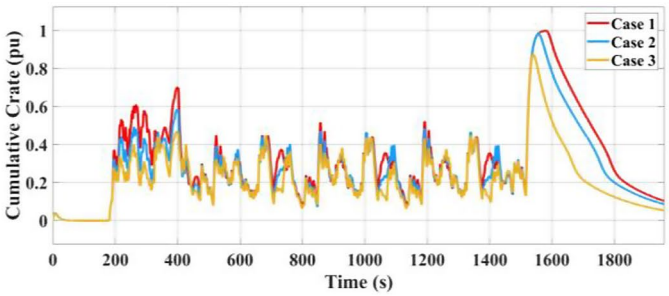

b)

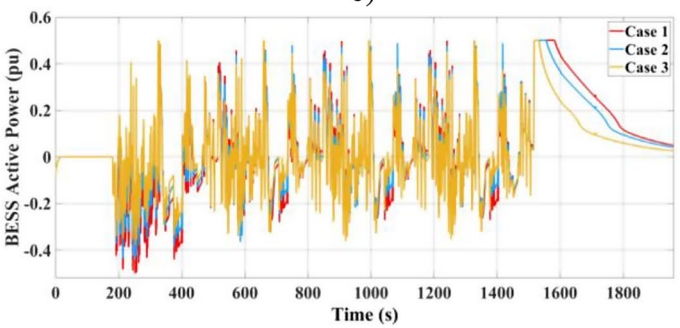

c)

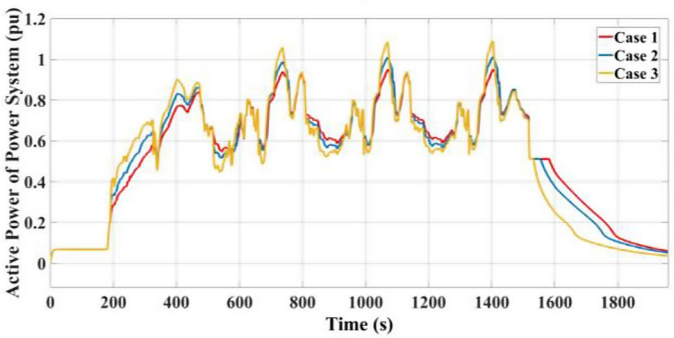

d)

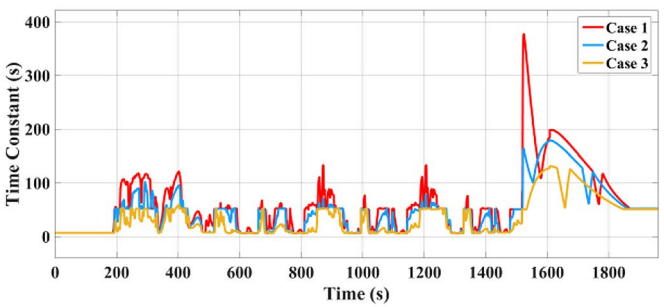

e)

Fig. 16 System behaviour using a fuzzy adaptive compensator: (**a**) frequency of power system, (**b**) cumulative *C-rate*, (**c**) BESS active power, (**d**) active power behaviour of the power system, (**e**) behaviour of the adaptive time constant

Table 5 Overall results of the performance with BESS and fuzzy-based adaptive compensator

Parameters	LPF with Fuzzy System		
	Case 1	Case 2	Case 3
Average power (pu)	0.152	0.135	0.112
Maximum frequency (Hz)	60.280	60.185	60.162
Minimum frequency (Hz)	59.741	59.757	59.772
Time above 60.2 Hz (s)	33	0	0
Time below 59.7 Hz (s)	0	0	0
Average cumulative C-rate (pu)	0.304	0.268	0.222
Charge Energy (MWh)	2.736	2.481	1.927
Discharge Energy (MWh)	1.711	1.446	1.287
FCE/a	867	766	627
ΔSOC (%)	17.84	15.49	9.67
$RoCoF_m$ (Hz/s)	0.120	0.105	0.061

In terms of the maximum rate of change of the frequency, the results obtained for the different control systems remain within the safety limits established by the various international standards [38, 39].

In relation to the charging and discharging energy of the battery, the behaviour remains similar in all cases with the non-adaptive compensator. These outcomes are notably superior compared to those obtained with the proposed FLC, as the adaptive control allows the battery to be charged or discharged depending on the conditions of the grid and the EAF, in conjunction with minimising the battery usage.

5.2 BESS SOC Dynamics for a Daily EAF Power Demand Profile

The previous sections analysed the behaviour of the BESS when operating a single EAF melting basket considered as reference. However, the production process is continuous, and, under real operating conditions, the number of baskets processed varies daily. In this context, it is essential to control the *SOC* of the BESS, as its adequate recovery is a fundamental requirement to ensure the sustained, reliable and long-term operation of the storage system. As detailed in Sect. 3.1, the proposed BESS control solution includes a *SOC* restoration controller that is activated during the break times between baskets.

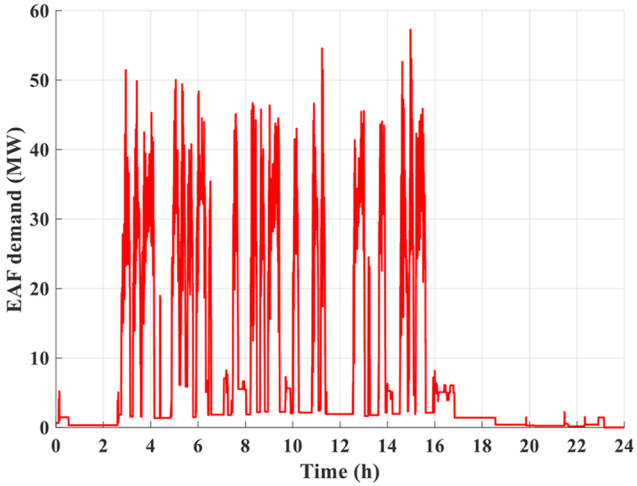

Fig. 17 Daily EAF power demand in the Cuban power system

Under these premises, further research was conducted in which multiple daily records of the actual demand of an EAF were collected under operating conditions like those analysed in previous sections. Figure 17 shows one demand record corresponding to a summer day in 2024, which is used as a case study to evaluate the BESS's *SOC* management. The demand record in question corresponds to the start of EAF smelting operations during the early morning hours (3:00 AM), when demand on the electrical system is lower. These operations continue into the afternoon to avoid coinciding with peak demand on the power system. This operating condition is particular in Cuba, being imposed by the system operator due to the current weakness of power system, to preserve frequency stability, and is consistent

Table 6 Comparison between the different control systems used in the EAF compensation BESS for the different case studies

Parameters	Case 1		Case 2		Case 3	
	LPF with Ts = 150 s	LPF with Fuzzy System	LPF with Ts = 150 s	LPF with Fuzzy System	LPF with Ts = 150 s	LPF with Fuzzy System
Average power (pu)	0.196	0.152	0.197	0.135	0.196	0.112
Maximum frequency (Hz)	60.248	60.280	60.172	60.185	60.130	60.162
Minimum frequency (Hz)	59.722	59.741	59.770	59.757	59.832	59.772
Time above 60.2 Hz (s)	66.612	33.461	0	0	0	0
Time below 59.7 Hz (s)	0	0	0	0	0	0
Average cumulative C-rate (pu)	0.384	0.304	0.385	0.268	0.384	0.222
Charge Energy (MWh)	2.632	2.736	2.632	2.481	2.632	1.927
Discharge Energy (MWh)	2.795	1.711	2.795	1.446	2.795	1.287
FCE/a	1058	867	1058	766	1058	627
ΔSOC (%)	16.82	17.84	16.82	15.49	16.82	9.67
$RoCoF_m$ (Hz/s)	0.097	0.120	0.090	0.105	0.052	0.061

with the operating conditions under which the demand records analysed in this study were collected.

The analysis of the SOC over the course of one day, under the conditions described above, was organised into five case studies, synthesized in Table 7. Both the initial state of charge of the battery (SOC_i) and the target *SOC* restoration (SOC^*), were varied. In the case of SOC^*, it is widely accepted that an optimal range is between 50 and 60%, as this provides sufficient energy reserves to respond to unexpected events, such as sudden changes in demand or requirements to support the electrical system.

However, in this study, the *SOC* reference value was not kept fixed, but was adjusted, considering that the industry can modify this parameter depending on daily operating conditions, the energy management strategy adopted, and the level of energy reserve required to ensure the continuity of the production process and the provision of auxiliary services. This flexibility in defining the reference *SOC* allows for more efficient operation of the storage system by balancing power availability, contingency response capacity, and battery life extension. Furthermore, various SOC_i values were considered to account for different SOC restoration levels that may occur from the previous day. Figure 18 shows the daily SOC evolution of the BESS for the five cases analysed.

As shown in Fig. 18, in Case 1, the *SOC* of the BESS approaches 100% at the end of the operating day, thereby limiting the availability of the storage system to adequately meet the demand of the subsequent EAF baskets. In contrast, in Cases 2 to 5, the *SOC* systematically returns to its reference value at the end of the day, ensuring that the battery is in proper operating condition for the next production cycle. These results demonstrate the long-term effectiveness of the *SOC* control strategy.

Table 7 BESS SOC parameters for different operating cases

Case no.	SOC controller status	SOC_i	SOC*
Case 1	Disabled	60%	60%
Case 2	Enabled	60%	60%
Case 3	Enabled	50%	70%
Case 4	Enabled	70%	80%
Case 5	Enabled	60%	50%

6 Experimental Validations

In this section, the BESS's converter control is validated experimentally through a laboratory-scale Power Hardware-in-the-loop (PHIL) testbench. Figure 19 shows the PHIL setup (block diagram and laboratory picture), highlighting the hardware and emulated parts. The BESS comprises of a 5 kW three-phase inverter, with an LC output filter, and a 650 V DC power supply that allows bidirectional power flow to emulate the battery. The inverter is connected to a four-quadrant power converter (FQPC), which is used to replicate the power system dynamics, according to the model presented in Sect. 3.

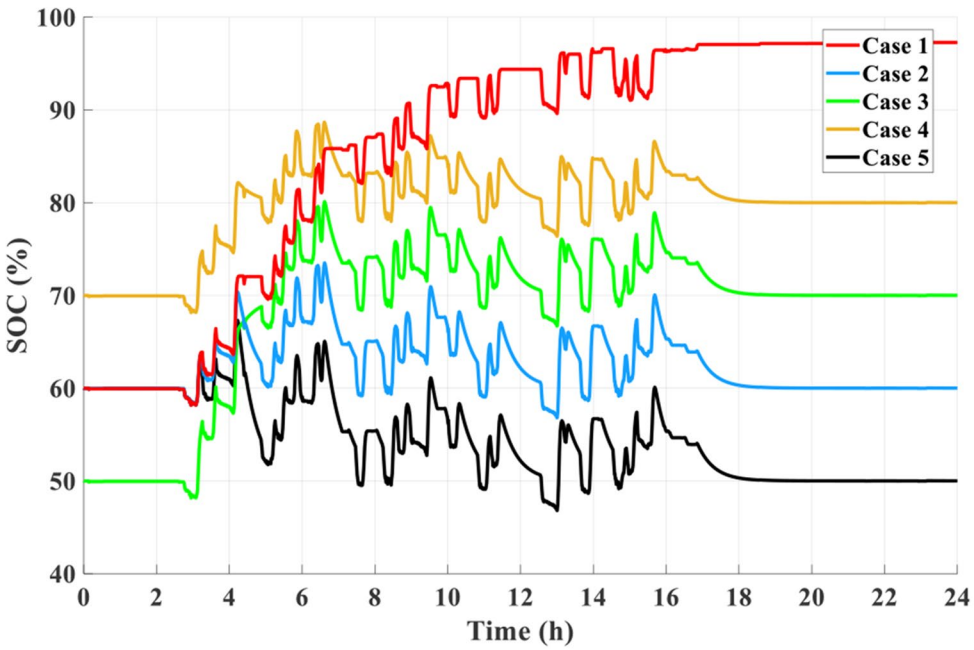

Fig. 18 Daily SOC variation of the BESS for the considered cases

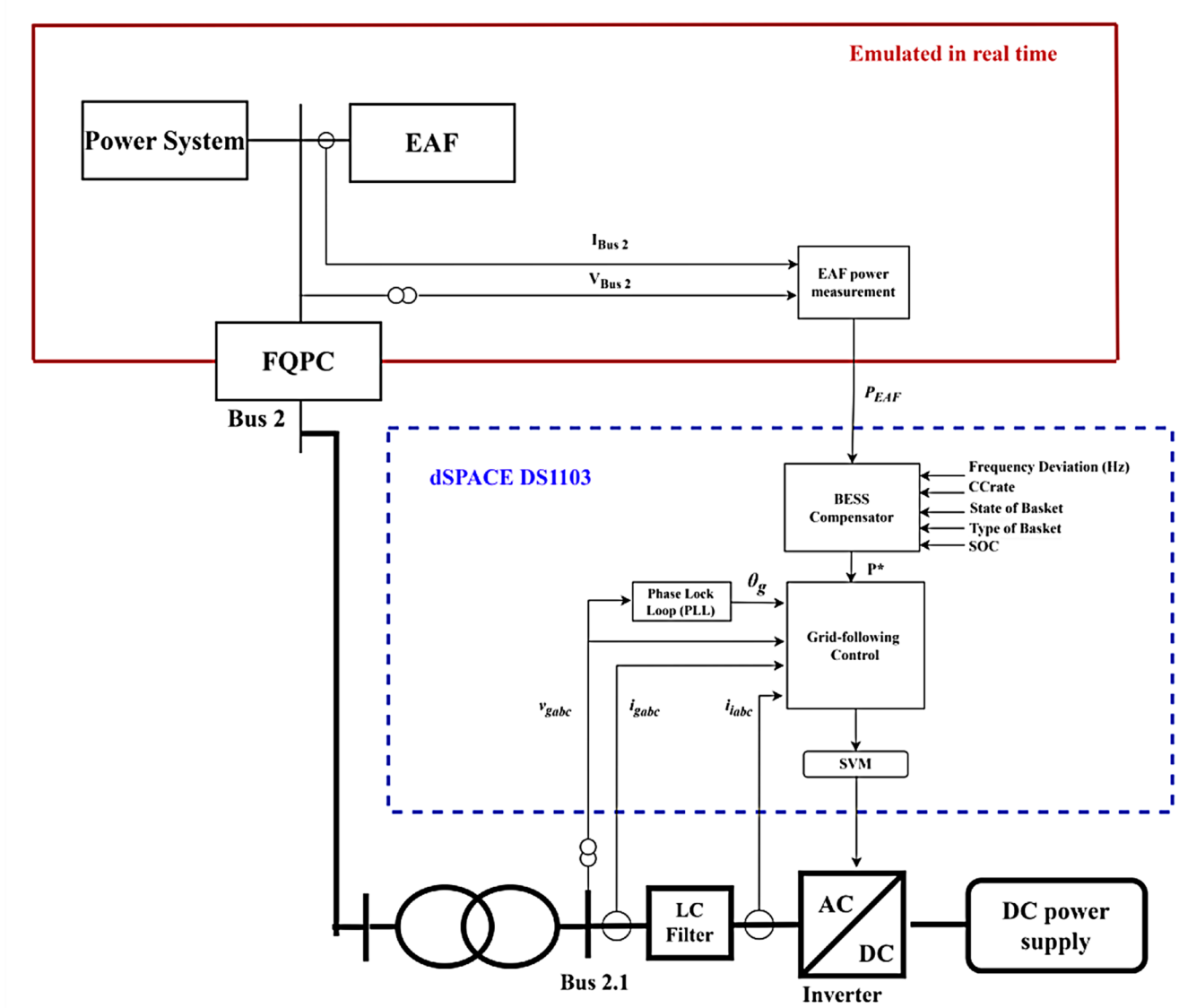

Fig. 19 PHIL setup: (**a**) block diagram; (**b**) laboratory illustration

Table 8 Main parameters of the experimental setup

Parameters	Values
Inverter rated power	5 kW
FQPC rated power	10 kW
Rated AC voltage	400 V
Rated frequency	60 Hz
DC inverter voltage	650 V
PWM switching frequency	10 kHz
Filter inductance	3 mH
Filter capacitance (star-connected)	10 μF

Along with the power system, the EAF is emulated within the FQPC, as highlighted in Fig. 19a. The main setup parameters are listed in Table 8. The BESS control discussed in Sect. 5 is implemented using a dSPACE DS1103 board, with data acquisition handled through dSPACE/ControlDesk software.

The main purpose of the experimental tests is to demonstrate the feasibility of implementing the proposed FLC. The following experimental results are obtained for one of the most severe scenarios we considered in Sect. 5, with the power system inertia of 58 MWs^2/rad and damping constant of 25 MW/rad/s. Figure 20 shows the main experimental results, including the active powers of the EAF and BESS, as well as the power system frequency. The base value for active powers representation in p.u. was 10 kW for the real power, and 50 MW for emulated power. Additionally, the variation of the filter's time constant (T_s), as provided by the FLC, and the battery's CC_{rate} are shown.

Table 9 shows a comparison between the simulation and experimental results, based on previously introduced performance indices. As shown, all values are close, with the largest difference observed in the time the frequency exceeds the upper bound of 60.2 Hz during the furnace high rate of power reduction at the end of the smelting process. Regarding the frequency excursion, both experimental and simulation results show that the frequency consistently remains above 59.7 Hz throughout the entire process, thus achieving the primary objective. Although the experimental results show that the frequency exceeds the 60.2 Hz threshold for a longer duration, as previously explained, this situation poses less risk to the stability of the Cuban power system. The filter's time constant (T_s) governed by the FLC remains below the reference value of 150 s for most of the time. However, during periods when the frequency approaches the upper or lower limits - at the beginning and end of the EAF process - the time constant is increased to enhance the BESS response and better compensate for the high-power ramp of the EAF. The effect of the FLC is also evident in the variation of the CC_{rate}, proving that the FLC contributes to reducing the battery stress.

7 Conclusions

This paper presented a fuzzy logic-based adaptive control system for a BESS designed to minimise the frequency deviations caused by a high-power EAF in the Cuban power system. The developed system compensates for the power demanded by the EAF based on the smoothing methods typically used in conjunction with renewable sources to limit the power ramp rate. Unlike the use of a non-adaptive compensator, which works similarly in all power system conditions, the FLC also reduces the work of the batteries. To quantify the BESS usage, the cumulative *C-rate* metric was introduced, and the results showed that its average value was lower in all cases where the BESS worked with the FLC compared to the non-adaptive compensator. In addition to reducing the work of the batteries, the FLC manages to control the frequency deviations by reducing the time the frequency is out of the dead band compared to the non-adaptive compensator. The results obtained from the FLC were experimentally validated using a laboratory-scale Power Hardware-in-the-Loop (PHIL) testbench, where it was confirmed that the experimental results were very similar to the values obtained from the simulations, thus demonstrating the feasibility of the solution shown in this research. In general, the results of this work showed that the implementation of an adaptive filter that considers the conditions of the power system, the EAF and the battery of a BESS provide a performant solution for steelworks connected to weak power systems, as is the current state of the Cuban power system.

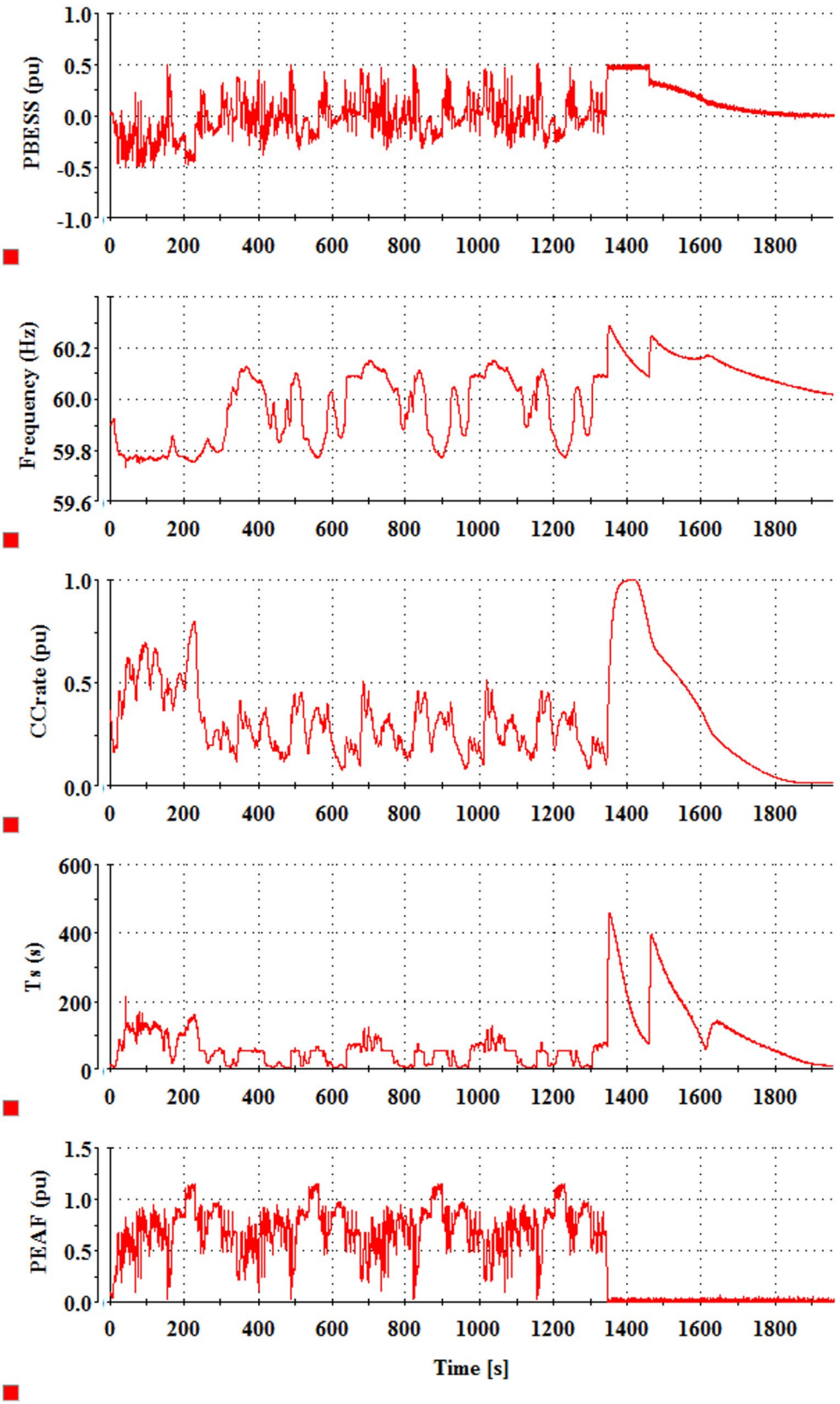

Fig. 20 Experimental results for the most challenging scenario (Case 1)

Table 9 Comparison between simulation and experimental results for the most challenging scenario (Case 1)

Parameters	Simulation Results	Experimental Results
Average power (p.u.)	0.152	0.157
Maximum frequency (Hz)	60.280	60.286
Minimum frequency (Hz)	59.741	59.731
Time above 60.2 Hz (s)	33.461	73
Time below 59.7 Hz (s)	0	0
Average cumulative C-rate (pu)	0.304	0.316

Author Contributions Julio Espinosa Domínguez: Writing – original draft, Validation, Software, Methodology, Investigation, Formal analysis, Conceptualization. Ioan Serban: Writing – review & editing, Validation, Supervision, Resources. Orlys Ernesto Torres Breffe: Writing – review & editing, Validation, Supervision.

Funding No funding was received to assist with the preparation of this manuscript.

Data Availability Data will be made available on request.

Declarations

Competing Interests The authors declare that they have no known competing financial interests or personal relationships that could have appeared to influence the work reported in this paper.

References

1. Abadi MM, Tang H, Rashidi MM (2024) A review of simulation and numerical modeling of electric arc furnace (EAF) and its processes. Heliyon 10(11):e32157. https://doi.org/10.1016/j.heliyon.2024.e32157
2. Łukasik Z, Olczykowski Z (2020) Estimating the impact of arc furnaces on the quality of power in supply systems. Energies 13(6):13. https://doi.org/10.3390/en13061462
3. Andrei H, Cepisca C, Grigorescu S (2011) Power quality and electrical arc furnaces. https://doi.org/10.5772/15996
4. Dominguez JE, Rekola J, Torres Breffe OE, Capablanca CR (2021) Use of battery energy storage with electric arc furnace to improve frequency stability of weak power system. In 2021 IEEE PES Innov Smart Grid Technol Eur ISGT Eur, pp 1–5. https://doi.org/10.1109/ISGTEurope52324.2021.9640151
5. Domínguez JE, Torres Breffe OE, Serban I, González CB, Revuelta Capablanca C (2023) The impact of electric arc furnaces on the Cuban power system: existing approaches and future prospects. In 2023 Int Symp Fundam Electr Eng ISFEE, pp 1–6. https://doi.org/10.1109/ISFEE60884.2023.10637080
6. Domínguez JE, Serban I, Breffe OET (2025) Adaptive voltage fault ride-through control of a battery energy storage system according to the cuban grid code. Energy 360 4:100033. https://doi.org/10.1016/j.energ.2025.100033
7. Farivar GG, Manalastas W, Tafti HD, Ceballos S, Sanchez-Ruiz A, Lovell EC et al. (2023) Grid-connected energy storage systems: state-of-the-art and emerging technologies. Proc IEEE 111(4):397–420. https://doi.org/10.1109/JPROC.2022.3183289
8. Prakash K, Ali M, Siddique MNI, Chand AA, Kumar NM, Dong D et al. (2022) A review of battery energy storage systems for ancillary services in distribution grids: current status, challenges and future directions. Front Energy Res 10:10. https://doi.org/10.3389/fenrg.2022.971704
9. Kim W-J, Lee Y-S, Chun Y-H (2020) Assessment of primary control reserve requirement from generator considering a battery energy storage system. J Electr Eng Technol 15(1):315–324. https://doi.org/10.1007/s42835-019-00319-2
10. Stein K, Tun M, Musser K, Rocheleau R (2018) Evaluation of a 1 MW, 250 kW-hr battery energy storage system for grid services for the island of Hawaii. Energies 11(12):3367. https://doi.org/10.3390/en11123367
11. Gamage D, Wanigasekara C, Ukil A, Swain A (2025) Multi-level consensus based load frequency controller with multi-battery energy storage systems. Electr Power Syst Res 239:111208. https://doi.org/10.1016/j.epsr.2024.111208
12. Saldarini A, Longo M, Brenna M, Zaninelli D (2023) Battery electric storage systems: advances, challenges, and market trends. Energies 16(22):7566. https://doi.org/10.3390/en16227566
13. Sukumar S, Marsadek M, Agileswari KR, Mokhlis H (2018) Ramp-rate control smoothing methods to control output power fluctuations from solar photovoltaic (PV) sources-A review. J Energy Storage 20:218–229. https://doi.org/10.1016/j.est.2018.09.013
14. Ochoa D, Martinez S, Arévalo P (2023) A novel fuzzy-logic-based control strategy for power smoothing in high-wind penetrated power systems and its validation in a microgrid lab. Electronics 12(7):1721. https://doi.org/10.3390/electronics12071721
15. Atif A, Khalid M (2020) Fuzzy logic controller for solar power smoothing based on controlled battery energy storage and varying low pass filter. IET Renew Power Gener 14(18):3824–3833. https://doi.org/10.1049/iet-rpg.2020.0459
16. Yan HW, Farivar GG, Beniwal N, Tafti HD, Ceballos S, Pou J et al. (2023) Battery lifetime extension in a stand-alone microgrid with flexible power point tracking of photovoltaic system. IEEE J Emerg Sel Top Power Electron 11(2):2281–2290. https://doi.org/10.1109/JESTPE.2022.3212702
17. Hassanzadeh ME, Nayeripour M, Hasanvand S, Waffenschmidt E (2022) Intelligent fuzzy control strategy for battery energy storage system considering frequency support, SoC management, and C-rate protection. J Energy Storage 52:104851. https://doi.org/10.1016/j.est.2022.104851
18. Akpinar KN, Gundogdu B, Ozgonenel O, Gezegin C (2023) An intelligent power management controller for grid-connected battery energy storage systems for frequency response service: a battery cycle life approach. Electr Power Syst Res 216:109040. https://doi.org/10.1016/j.epsr.2022.109040
19. MdR A, Bhuiyan I, Mohammad N (2023) A feasibility study of solar photovoltaic power smoothing using fuzzy logic approach. J Sustain Energy 14:124–135

20. Tephiruk N, Kanokbannakorn W, Kerdphol T, Mitani Y, Hongesombut K (2018) Fuzzy logic control of a battery energy storage system for stability improvement in an islanded Microgrid. Sustainability 10(5):1645. https://doi.org/10.3390/su10051645
21. Syed MA, Khalid M (2021) Neural network predictive control for smoothing of solar power fluctuations with battery energy storage. J Energy Storage 42:103014. https://doi.org/10.1016/j.est.2021.103014
22. Cano A, Arévalo P, Jurado F (2024) Neural network predictive control in renewable systems (HKT-PV) for delivered power smoothing. J Energy Storage 87:111332. https://doi.org/10.1016/j.est.2024.111332
23. Al-Hinai A, Alyammahi H, Haes Alhelou H (2021) Coordinated intelligent frequency control incorporating battery energy storage system, minimum variable contribution of demand response, and variable load damping coefficient in isolated power systems. Energy Rep 7:8030–8041. https://doi.org/10.1016/j.egyr.2021.07.072
24. Virulkar V, Aware MV (2009) Reactive and real power compensation with DSTATCOM and BESS for mitigation of flicker. Int J Power Energy Convers 1(4):384. https://doi.org/10.1504/IJPEC.2009.029055
25. Toopchizadeh H, Zallaghi M, Moradi M, Shahmoradi S (2023) An effective shunt active power filter based on novel binary multilevel inverter and optimal type-2 fuzzy system to accurately mitigate harmonic currents. Evol Syst 14(5):783–800. https://doi.org/10.1007/s12530-022-09465-x
26. Virulkar VB, Aware MV (2008) DSTATCOM with BESS, an efficient means for flicker mitigation. In TENCON, 2008 – 2008 IEEE Reg 10 Conf, pp 1–6. https://doi.org/10.1109/TENCON.2008.4766740
27. Orcajo GA, Cano JM, Norniella JG, FP G, Rojas CH, JR D (2023) Hybridization of a wind farm and a photovoltaic plant in a steelworks with an energy storage system. In 2023 IEEE Ind Appl Soc Annu Meet, IAS, pp. 1–7. https://doi.org/10.1109/IAS54024.2023.10406767
28. Fahren A, Banjar Nahor K, Widjaja CD, Hariyanto N (2020) Static watt compensator and battery energy storage system for frequency stability considering smelter: a comparison. https://doi.org/10.1109/PECon48942.2020.9314465
29. 2009). European network of transmission system operators for electricity (ENTSO-e). P1 - policy, 1 [Load-Frequency Control and Performance [C]
30. Xu Z, Qin Y, Li Z, Jiao C, Zhai B, Chang X (2023) Stability analysis of different control modes of grid-connected converters under different grid conditions. Front Energy Res 11. https://doi.org/10.3389/fenrg.2023.1242024
31. Aljarrah R, Fawaz BB, Salem Q, Karimi M, Marzooghi H, Azizipanah-Abarghooee R (2024) Issues and challenges of grid-following converters interfacing renewable energy sources in low inertia systems: a review. IEEE Access 12:5534–5561. https://doi.org/10.1109/ACCESS.2024.3349630
32. Shehata EG, Gaber MS, Ahmed KA, Salama GM (2019) Implementation of an energy management algorithm in DC MGs using multi-agent system. Int Trans Electr Energy Syst 29(4):e2790. https://doi.org/10.1002/etep.2790
33. Domínguez JE, Serban I, Breffe OET (2024) Enhancing the control of a DC/AC converter for voltage perturbation ride-through in compliance with the Cuban grid code. In 2024 6th Glob. Power Energy Commun. Conf. GPECOM, pp 68–73. https://doi.org/10.1109/GPECOM61896.2024.10582679
34. ABB Company (n.d.) PCS100 ESS grid connect interface for Energy storage systems user manual
35. Kundur P, Balu NJ (1994) Power system stability and control. McGraw-Hill
36. Kolacia T, Drapela J (2016) Voltage sensitivity to power flows related to distributed generation. In 2016 17th Int Sci Conf Electr Power Eng EPE, pp 1–6. https://doi.org/10.1109/EPE.2016.7521809
37. Wang G, Huang Y, Xu Z (2024) Voltage stiffness for strength evaluation of VSC-penetrated power systems. IEEE Trans Power Syst 39(4):6119–6122. https://doi.org/10.1109/TPWRS.2024.3388250
38. Deng X, Mo R, Wang P, Chen J, Nan D, Liu M (2023) Review of RoCoF estimation techniques for low-inertia power systems. Energies 16(9):3708. https://doi.org/10.3390/en16093708
39. Prabhakar K, Jain SK, Padhy PK (2022) Inertia estimation in modern power system: a comprehensive review. Electr Power Syst Res 211:108222. https://doi.org/10.1016/j.epsr.2022.108222
40. Fleer J, Stenzel P (2016) Impact analysis of different operation strategies for battery energy storage systems providing primary control reserve. J Energy Storage 8:320–338. https://doi.org/10.1016/j.est.2016.02.003
41. Kovačič M, Stopar K, Vertnik R, Šarler B (2019) Comprehensive electric arc furnace electric energy consumption modeling: a pilot study. Energies 12(11):2142. https://doi.org/10.3390/en12112142

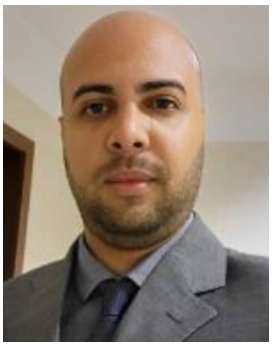

Julio Espinosa Domínguez was born in Cuba, in 1993. He received his B.Sc. and M.Sc. degrees in Electrical Engineering from the Technological University of Havana, Cuba, in 2018 and 2022, respectively. Currently, he is a Ph.D. student within the Department of Electrical Engineering and Applied Physics at the Transilvania University of Brasov, Romania. His research focuses on power electronics applied to the industrial sector.

Ioan Serban (Member, IEEE) was born in Romania, in 1981. He received the B.Sc. and Ph.D. degrees in electrical engineering from Transilvania University of Brasov, Brasov, Romania, in 2004 and 2008, respectively. He is currently a Full Professor with the Department of Electrical Engineering and Applied Physics, Faculty of Electrical Engineering and Computers Science, Transilvania University of Brasov. His research interests include power converters for interfacing renewable energy sources, and energy storage systems for grid and microgrid applications. Prof. Serban was the recipient of the 2015 IET Renewable Power Generation Premium Award. Over the past five years, he has been included in the Stanford University/Elsevier World's Top 2% Scientists list.

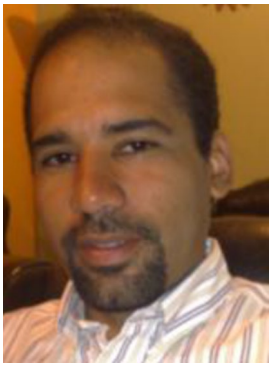

Orlys Ernesto Torres Breffe was born in Cuba, in 1972. He received his B.Sc. degree in Electrical Engineering from the University of Moa in 1995, an M.Sc. degree from the University of Camagüey in 1999, and a Ph.D. in Technical Sciences from the José Antonio Echeverría Higher Polytechnic Institute (CUJAE) in 2005. He is currently a Full Professor within the Department of Electrical Engineering at the Technological University of Havana. He also serves as the Coordinator for Graduate Diplomas in Electrical Protection. His research interests include power systems, electrical protection, stability, the application of power electronics in electric arc furnaces, and the protection of generator sets.